AMERICAN SOCIETY FOR MICROBIOLOGY | Journal of Virology®

PATHOGENESIS AND IMMUNITY

Increased Sensitivity of SARS-CoV-2 to Type III Interferon in Human Intestinal Epithelial Cells

Camila Metz-Zumaran,[a] Carmon Kee,[a,b] Patricio Doldan,[a,b] Cuncai Guo,[a] Megan L. Stanifer,[c,d] Steeve Boulant[a,b,d]

[a]Department of Infectious Diseases, Virology, Heidelberg University, Heidelberg, Germany
[b]Research Group "Cellular Polarity and Viral Infection," German Cancer Research Center (DKFZ), Heidelberg, Germany
[c]Department of Infectious Diseases, Molecular Virology, Heidelberg University, Heidelberg, Germany
[d]Department of Molecular Genetics and Microbiology, College of Medicine, University of Florida, Gainesville, Florida, USA

Camila Metz-Zumaran, Carmon Kee, and Patricio Doldan contributed equally to this article. Author order was determined by all three co-authors and agreed by the corresponding authors.

ABSTRACT The coronavirus SARS-CoV-2 caused the COVID-19 global pandemic leading to 5.3 million deaths worldwide as of December 2021. The human intestine was found to be a major viral target which could have a strong impact on virus spread and pathogenesis since it is one of the largest organs. While type I interferons (IFNs) are key cytokines acting against systemic virus spread, in the human intestine type III IFNs play a major role by restricting virus infection and dissemination without disturbing homeostasis. Recent studies showed that both type I and III IFNs can inhibit SARS-CoV-2 infection, but it is not clear whether one IFN controls SARS-CoV-2 infection of the human intestine better or with a faster kinetics. In this study, we could show that type I and III IFNs both possess antiviral activity against SARS-CoV-2 in human intestinal epithelial cells (hIECs); however, type III IFN is more potent. Shorter type III IFN pretreatment times and lower concentrations were required to efficiently reduce virus load compared to type I IFNs. Moreover, type III IFNs significantly inhibited SARS-CoV-2 even 4 h postinfection and induced a long-lasting antiviral effect in hIECs. Importantly, the sensitivity of SARS-CoV-2 to type III IFNs was virus specific since type III IFN did not control VSV infection as efficiently. Together, these results suggest that type III IFNs have a higher potential for IFN-based treatment of SARS-CoV-2 intestinal infection compared to type I IFNs.

IMPORTANCE SARS-CoV-2 infection is not restricted to the respiratory tract and a large number of COVID-19 patients experience gastrointestinal distress. Interferons are key molecules produced by the cell to combat virus infection. Here, we evaluated how two types of interferons (type I and III) can combat SARS-CoV-2 infection of human gut cells. We found that type III interferons were crucial to control SARS-CoV-2 infection when added both before and after infection. Importantly, type III interferons were also able to produce a long-lasting effect, as cells were protected from SARS-CoV-2 infection up to 72 h posttreatment. This study suggested an alternative treatment possibility for SARS-CoV-2 infection.

KEYWORDS SARS-CoV-2, human intestinal epithelial cells, interferon, intrinsic immune response, type III interferon, interferon lambda

Since the end of 2019 we have witnessed a global pandemic due to the emergence of the severe-acute-respiratory-syndrome-related coronavirus-2 (SARS-CoV-2) (1). Coronaviruses are enveloped, single-stranded positive-sense RNA viruses that can infect most animal species and generally cause common colds in humans (2). However, in the past 19 years coronaviruses have been involved in zoonotic events giving rise to highly pathogenic human viruses (e.g., MERS and SARS-CoV-1). The latest, SARS-CoV-2, is responsible for the coronavirus-associated acute respiratory disease or coronavirus disease 19 (COVID-19) and, as of December 2021, has caused more than 274 million infections and 5.3 million deaths

Editor Kanta Subbarao, The Peter Doherty Institute for Infection and Immunity

Address correspondence to Megan L. Stanifer, m.stanifer@ufl.edu, or Steeve Boulant, s.boulant@ufl.edu.

The authors declare no conflict of interest.

Received 5 October 2021
Accepted 28 January 2022
Published 9 March 2022

worldwide (World Health Organization, 2021). The virus and its associated disease have caused a worldwide medical and economic impact and united efforts are necessary to find adequate antiviral treatments.

The spread of the virus among humans is thought to occur through respiratory droplets. In this way, SARS-CoV-2 primarily targets cells of the airway epithelium, causing respiratory symptoms ranging from cough and shortness of breath to severe lung injury (3, 4). Interestingly, a significant number of patients with COVID-19 report gastrointestinal symptoms, including diarrhea, nausea, or vomiting, that can either precede or follow respiratory symptoms (3, 5–7). Moreover, multiple reports detected viral RNA in feces, and stool specimens of infected patients remained positive even after a negative oropharyngeal swab test (8–13). Direct evidence for viral infection of gut tissue was also shown through evaluation of endoscopic samples (7, 10, 14). Importantly, in recent months the understanding of intestinal SARS-CoV-2 infection and pathogenesis was improved with *in vitro* studies. Several studies demonstrated that immortalized human intestinal cells and primary human minigut organoids supported SARS-CoV-2 infection (15–18). Altogether, the medical reports and scientific data clearly show that SARS-CoV-2 is not restricted to the respiratory tract but can infect the human intestinal epithelium. However, the extent to which the enteric phase is important for viremia, pathogenesis, and transmission remains unknown.

Most cells in the body respond to viral infection by generating both a proinflammatory and an interferon (IFN) response. Secreted IFNs bind to IFN receptors inducing a signaling cascade, leading to the transcription of hundreds of interferon-stimulated genes (ISGs), which in turn create an antiviral state (19). Almost all cells in the body produce and respond to type I IFN to mount their antiviral response. Interestingly, the response of both lung and intestinal epithelial cells to viral infection also strongly depends on an additional interferon, the type III IFN. This tropism for the type III IFN action is due to the fact that the type III IFN receptor is mainly expressed on epithelial cells, placing it as a unique antiviral strategy for epithelium and mucosal surfaces. Several studies have demonstrated that during enteric virus infection, the type I IFNs are essential to protect against systemic spread, while the type III IFNs maintain epithelial balance protecting intestinal epithelial cells while limiting an exacerbated immune response (20–26), and this observation also stands true for lung respiratory epithelium (27, 28). Importantly, while human intestinal epithelial cells can respond to both type I and III IFNs to control virus replication and spread when exogenously provided (16, 29, 30), evidence suggests that the endogenous type III IFN are key to protect against virus infection (31). The function of type I and III IFNs in the respiratory tract appears to be dependent on the location of the infection. Within the upper respiratory tract, type III IFNs are key to control influenza viruses (27), while in the lower airway epithelium, both type I and type III IFNs have redundant functions in controlling viral infection (32).

Infection of human lung epithelial cells by SARS-CoV-2 was reported to induce a typical IFN response shown by the upregulation of the IFN themselves as well as the induction of ISGs (33, 34). Interestingly, other reports described a limited to absent IFN response upon SARS-CoV-2 infection of lung epithelial cells (35–38), which could be the result of the mechanisms developed by SARS-CoV-2 to interfere with both the production of IFN and its downstream signaling (17, 39). The impact of SARS-CoV-2 on human intestinal epithelial cells is much less characterized compared to the lung epithelial cells; however, there is clear evidence showing that a typical type I and type III IFN intrinsic innate immune response is generated upon infection (15, 31, 36).

Treatment of both lung and intestinal epithelial cells with type I IFN was reported to partially protect against SARS-CoV-2 infection (34, 37, 38, 40–42). Similarly, pretreatment of epithelial cells with type III IFN was also reported to interfere with SARS-CoV-2 infection/replication (31, 38, 40, 43). Interestingly, SARS-CoV-2 infection of human intestinal organoids, revealed that upon infection, primary human intestinal epithelial cells favor the production and secretion of type III IFN (31). In addition, deletion of either the type I IFN receptor or the type III IFN receptor from human intestinal epithelial cells revealed that the type III IFNs rather than type I IFNs had a predominant role in controlling SARS-CoV-2 infection (31). The molecular origins

for this more important function of type III IFN in protecting against SARS-CoV-2 in human intestinal epithelial cells remains unclear.

While it is now clear that the human intestinal epithelium mounts an IFN-dependent response upon SARS-CoV-2 infection, there are very few data about the kinetics of IFN-mediated protection. In this study, we investigate in detail how type I and III IFNs establish their antiviral program against SARS-CoV-2 infection in human intestinal epithelial cells. Our results showed that endogenous type I IFNs play a minor role in inhibiting SARS-CoV-2 infection; however, over time, endogenous type III IFNs play an essential role in controlling virus spread. While both type I and III IFNs induced an antiviral activity against SARS-CoV-2 at high concentrations, low concentrations and shorter pretreatment of type III IFNs were sufficient to inhibit virus infection. The sensitivity of SARS-CoV-2 to type III IFNs is virus specific, since pretreatment of human intestinal epithelial cells with the same IFN concentrations and for the same amount of time did not have the same deleterious effect on VSV infection as on SARS-CoV-2 infection. Importantly, type III IFN were able to have a long-lasting effect, eliciting an antiviral state even 72h posttreatment, indicating that using type III IFNs as antiviral measures could have strong potential to clear infection and *de novo* virus shedding from the human intestine.

RESULTS

Endogenous type III IFNs control SARS-CoV-2 replication and spread in human intestinal epithelial cells. As growing evidence supports that the gastrointestinal tract can be infected by SARS-CoV-2, studying the antiviral immune response of human intestinal epithelial cells (hIECs) is essential to understand COVID-19 pathogenesis. Previous data demonstrated that SARS-CoV-2 infection induces an IFN-dependent immune response in hIECs (15, 31, 44). To recapitulate these findings, we infected human colon carcinoma T84 cells with SARS-CoV-2 at an MOI of 0.04 (as determined in Vero cells) and measured the activation of the IFN-mediated intrinsic innate immune response (Fig. 1). We found that SARS-CoV-2 induced both type I (IFN-β1) and type III (IFN-λ2/3) IFN transcription (Fig. 1A), and the secreted IFNs were readily detectable in the supernatant of infected cells (Fig. 1B). Moreover, at 24 h postinfection (hpi), an increase of STAT1 phosphorylation was observed, confirming the activation of the JAK-STAT signaling pathway (Fig. 1C). These data confirm that SARS-CoV-2 infection induces an IFN-dependent immune response in hIECs.

We previously reported that type III IFNs are critical to control SARS-CoV-2 infection in hIECs (31). This was further supported by the observation that knocking out the type III IFN receptor leads to a greater increase of SARS-CoV-2 infection, replication, and *de novo* virus production compared to the knockout of the type I IFN receptor (31). These previous findings were performed at a single time point after IFN treatment and only gave a static view of type III IFNs role in controlling SARS-CoV-2 infection. To address how type I and type III IFNs play a role in confining virus replication and spread over time in hIECs, we infected T84 wild-type cells or T84 cells depleted of the type I IFN receptor ($IFNAR^{-/-}$), the type III IFN receptor ($IFNLR^{-/-}$), or both IFN receptors (double knockout [dKO]) with SARS-CoV-2 at an MOI of 0.04 (as determined in Vero cells). At different times postinfection, the cells were fixed and immunostained with an antibody targeting the viral nucleocapsid protein (Fig. 2A). Results show that at early time postinfection (i.e., 4 and 8 hpi), cells depleted of the type I IFN receptor ($IFNAR^{-/-}$) and cells depleted of both IFN receptors (dKO) were slightly more infected compared to wild-type (WT) T84 cells and cells depleted of the type III IFN receptor (Fig. 2B). In contrast, at later times postinfection (i.e., 12 and 24 hpi), cells depleted of the type III IFN receptor were found to be more infectible compared to cells depleted of the type I IFN receptor (Fig. 2B). These findings confirm that both the type I and type III IFN systems are important to control SARS-CoV-2 infection in hIECs and suggest that both IFNs confer antiviral properties to hIECs with different kinetics.

To address whether virus replication was also increased in cells depleted of IFN receptors, T84 WT and IFN receptor knockout cells were infected with SARS-CoV-2, and virus replication was monitored over time by quantitative reverse transcription-PCR (qRT-PCR). In agreement with our previous findings (31), the results show that cells depleted of both IFN receptors supported a greater SARS-CoV-2 replication (Fig. 2C). Importantly, and similar to the

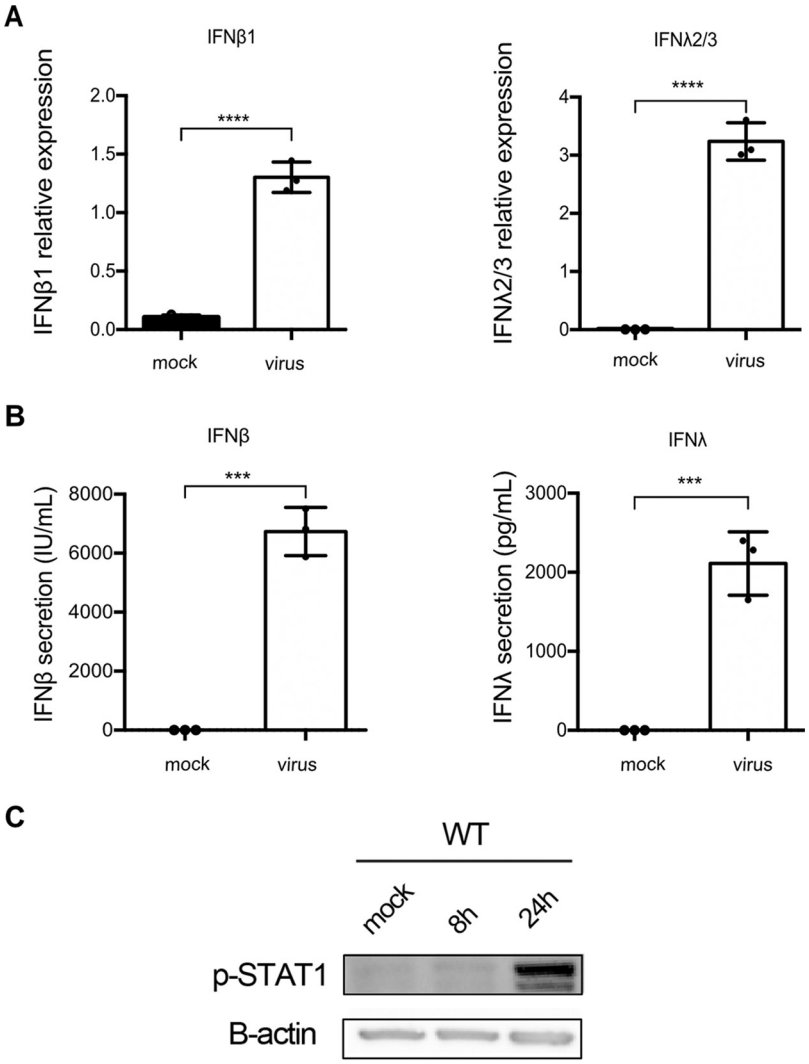

FIG 1 SARS-CoV-2 induces an IFN-dependent signaling cascade. (A to C) WT T84 cells were mock treated or infected with SARS-CoV-2 using an MOI of 0.04 (as determined in Vero cells). Cells were harvested at different time points postinfection, and the expression of IFNs and the activation of IFN-dependent signaling were determined. (A) At 24 hpi, the cell RNA was harvested to assess the IFN-β1 and IFN-λ2/3 relative expression using qRT-PCR. (B) At 24 hpi, the supernatants of infected cells were harvested, the infectious virus in the supernatant was inactivated, and the secretion of type I and III IFNs was assessed by the HEK-Blue assay. (C) At 8 and 24 hpi, the cells were lysed, and the activation of the JAK-STAT pathway was determined by STAT phosphorylation by Western blotting. FOr panles A and B, the error bars indicate the standard deviations (n = 3 biological replicates). ***, $P < 0.001$; ****, $P < 0.0001$ (as determined by a two-tailed unpaired t test with Welch's correlation).

number of infected cells (Fig. 2B), IFNLR$^{-/-}$ cells showed higher levels of viral copy number compared to WT T84 and IFNAR$^{-/-}$ cells at late times postinfection (Fig. 2C). Interestingly, at a late time postinfection (i.e., 24 hpi), IFNAR$^{-/-}$ cells show a similar level of SARS-CoV-2 replication compared to WT cells (Fig. 2C).

Finally, to test to which extent the absence of IFN signaling affects *de novo* virus production, T84 WT and IFN receptor knockout cells were infected with SARS-CoV-2. The supernatants of infected cells were harvested at 8, 12, and 24 hpi, and titers were determined on naive Vero cells to obtain the viral 50% tissue culture infective dose(s) ($TCID_{50}$)/mL present in the T84 cell supernatant. *De novo* virus production and release was greatly affected by intrinsic IFN signaling (Fig. 2D). Similar to our previous results on the number of infected cells and viral replication levels (Fig. 2B and C), dKO and IFNLR$^{-/-}$ cells showed a greater amount of *de novo* viral particles in the supernatant than WT T84 and IFNAR$^{-/-}$ cells (Fig. 2D). Altogether, our results confirm that the absence of IFN signaling favors SARS-CoV-2 infection, replication,

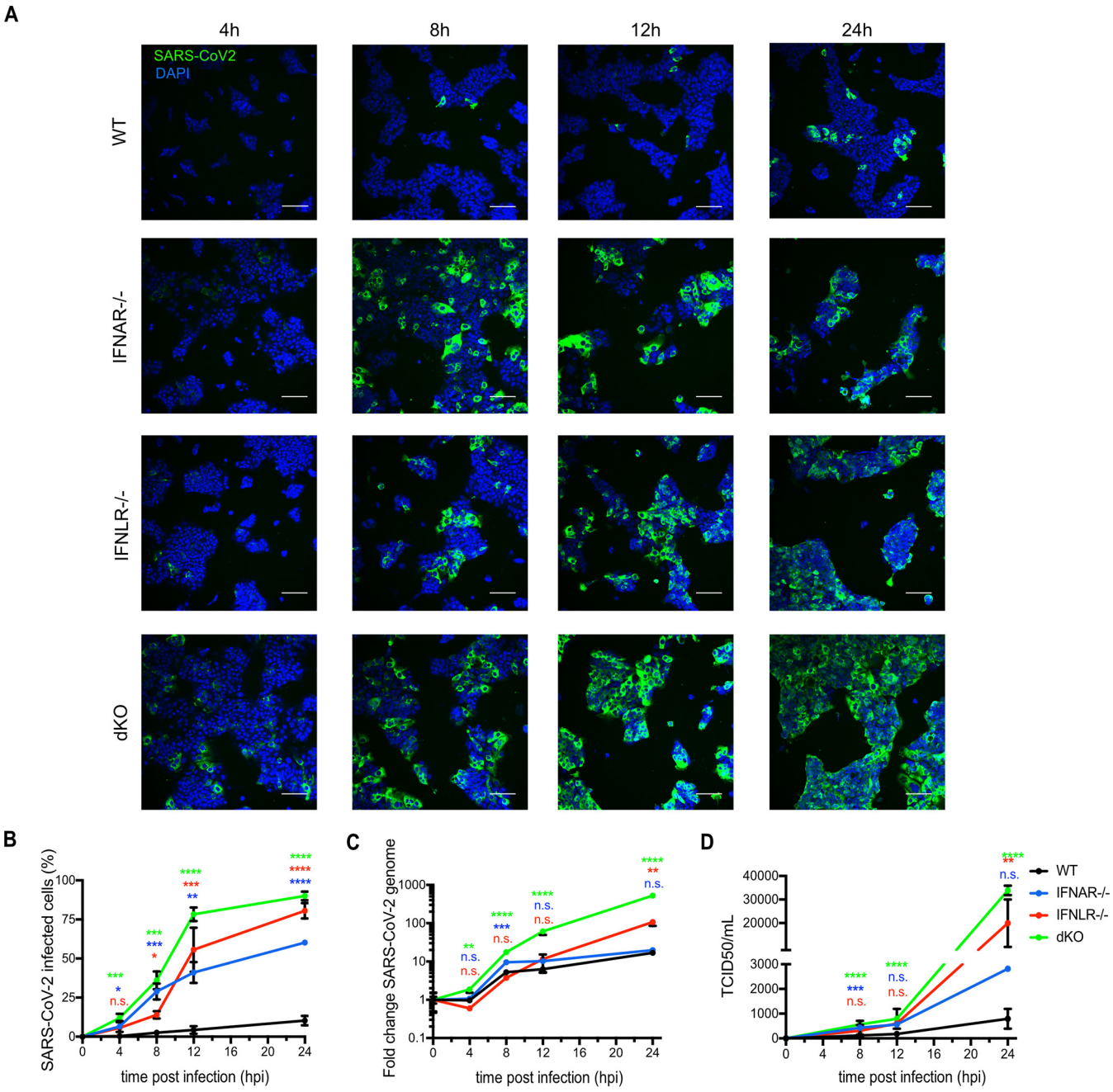

FIG 2 Kinetics of SARS-CoV-2 infection in human intestinal epithelial cells. (A to D) Wild-type T84 cells and T84 cells depleted of type I IFN receptor (IFNAR$^{-/-}$), type III IFN receptor (IFNLR$^{-/-}$), or both IFN receptors (dKO) were infected with SARS-CoV-2 at an MOI of 0.04 (as determined in Vero cells). At 0, 4, 8, 12, and 24 hpi, the cells were harvested to assess virus infection, replication, and *de novo* particle release. (A) Indirect immunofluorescence was performed against the viral nucleocapsid protein (green). Nuclei were stained with DAPI (blue). Representative images are shown. Scale bar, 100 μm. (B) Same as panel A except that the percentage of SARS-CoV-2-positive cells was quantified. (C) RNA was harvested, and qRT-PCR was used to evaluate the copy number of the SARS-CoV-2 genome. The data are normalized to input. (D) WT T84 supernatants for 0, 8, 12, and 24 hpi were harvested and titrated on Vero cells. After 24 h, Vero cells were fixed, and the $TCID_{50}$/mL of newly produced particles was determined by in-cell Western analyses using an antibody against the viral nucleocapsid. For panels B to D, error bars indicate the standard deviations (n = 3 biological replicates). n.s., not significant; *, $P < 0.05$; **, $P < 0.01$; ***, $P < 0.001$; ****, $P < 0.0001$ (as determined by an ordinary one-way ANOVA with Dunnett's multiple-comparison test using WT T84 cells as reference). The color of the significance stars represents the cell line that is being compared to WT T84 (green for dKO, red for IFNLR$^{-/-}$, and blue for IFNAR$^{-/-}$).

de novo particle production, and spread and that the type III IFN pathways appear to play a more fundamental protective function against SARS-CoV-2.

IFNs inhibit SARS-CoV-2 infection in a concentration-dependent manner. Our data show that endogenous type III IFN-mediated signaling is critical to control SARS-CoV-2 infection in hIECs, while endogenous type I IFNs may play a less important protective role.

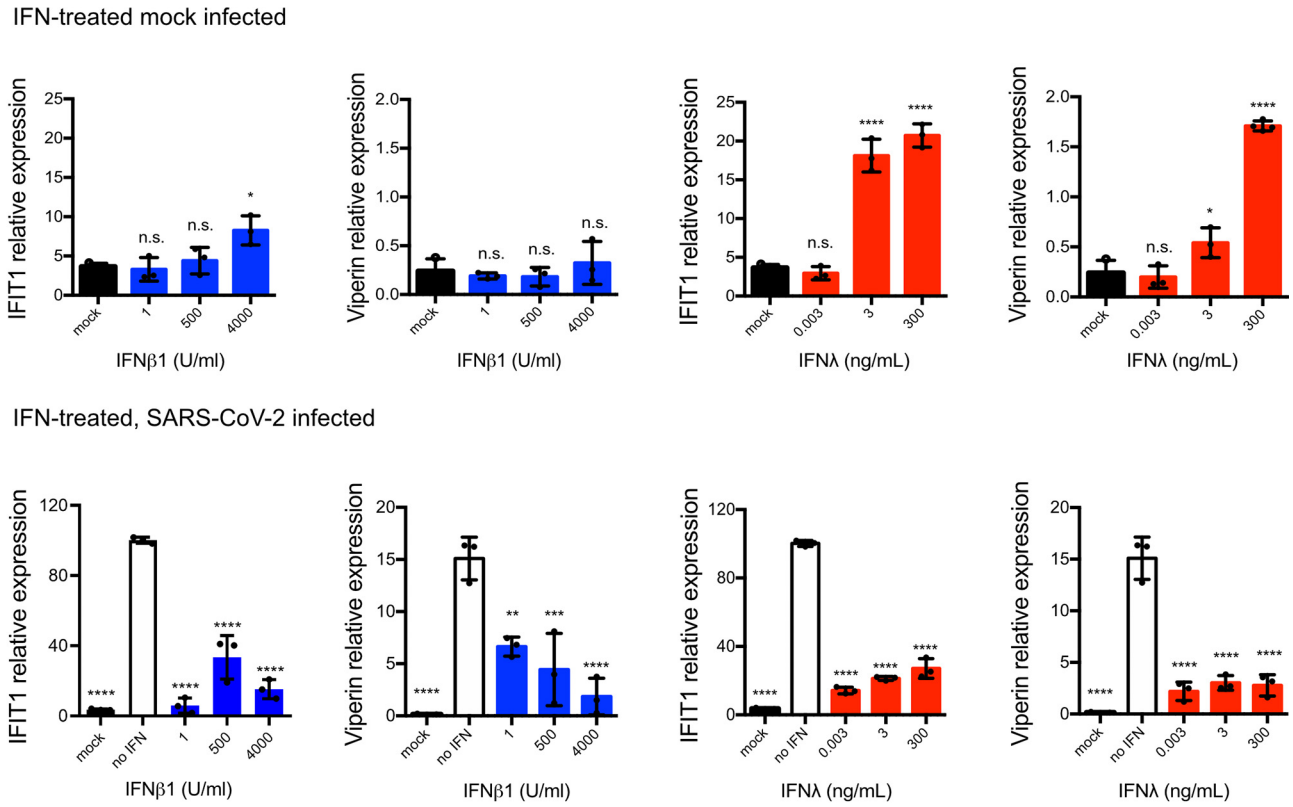

FIG 3 ISG expression of IFN-treated and SARS-CoV-2-infected WT T84 cells. (A and B) WT T84 cells were mock treated or pretreated with representative concentrations of type I (IFN-β1) and type III (IFN-λ1/2/3) IFNs for 24 h. The cells were either left uninfected (A) or were infected with SARS-CoV-2 using an MOI of 0.04 (B), and IFNs were maintained in the medium. At 24 hpi, RNA was harvested to assess the relative expression of IFN-stimulated genes (ISGs) IFIT1 and Viperin by qRT-PCR. Error bars indicate the standard deviations (n = 3 biological replicates). n.s., not significant; *, $P < 0.05$; **, $P < 0.01$; ***, $P < 0.001$; ****, $P < 0.0001$ (as determined by ordinary one-way ANOVA with Dunnett's multiple-comparison test using mock-treated [A] or nontreated infected [B] cells as a reference).

However, we and others have previously reported that both type I and type III IFNs mediate an antiviral protection and that both IFNs are able to restrict SARS-CoV-2 virus replication (29, 31, 40). In order to bypass the possibility that the differences at early times postinfection between the type I and III IFN receptor KO cell lines are due to type I IFNs being secreted faster than type III IFNs, we decided to synchronize the IFN-mediated response through exogenous treatment. Previous work from our group has shown that T84 cells are able to mount an IFN-dependent response upon treatment with either type I or type III IFNs (29). To confirm this, WT T84 cells were either mock treated or treated with different concentrations of type I (IFN-β1) and type III (λ1/2/3) IFNs. At 24 h posttreatment, RNA was harvested, and the ISG expression levels were measured. Both type I and III IFNs lead to a significant increase of IFIT1 expression compared to mock-treated samples (Fig. 3A) while Viperin expression was increased only with type III IFNs (Fig. 3A) at 24 h posttreatment. It is possible that type I IFNs induce a faster but short-lasting ISG activation, and thus at 24 h posttreatment the transcript levels are decaying. These differences between IFIT1 and Viperin were consistent with our previous work that show that type I and type III IFN induce similar ISGs but with different kinetics.

To directly test the efficiency of IFNs in controlling SARS-CoV-2 infection and to address whether type I and III IFNs have a different kinetics and efficiency of antiviral activity, WT T84 cells were either mock treated or pretreated with increasing concentrations of type I (IFN-β1) or type III (IFN-λ1/2/3) IFNs for 12 or 24 h prior to infection with SARS-CoV-2 at an MOI of 0.04 (as determined in Vero cells) (Fig. 4A). SARS-CoV-2 infection of cells pretreated with either type I or type III IFNs resulted in an increased induction of ISG expression (Fig. 3B) compared to IFN-treatment alone without infection (Fig. 3A), likely as a result of the cooperative effect of the IFN used to prestimulate the cells and the IFN produced by cells upon infection.

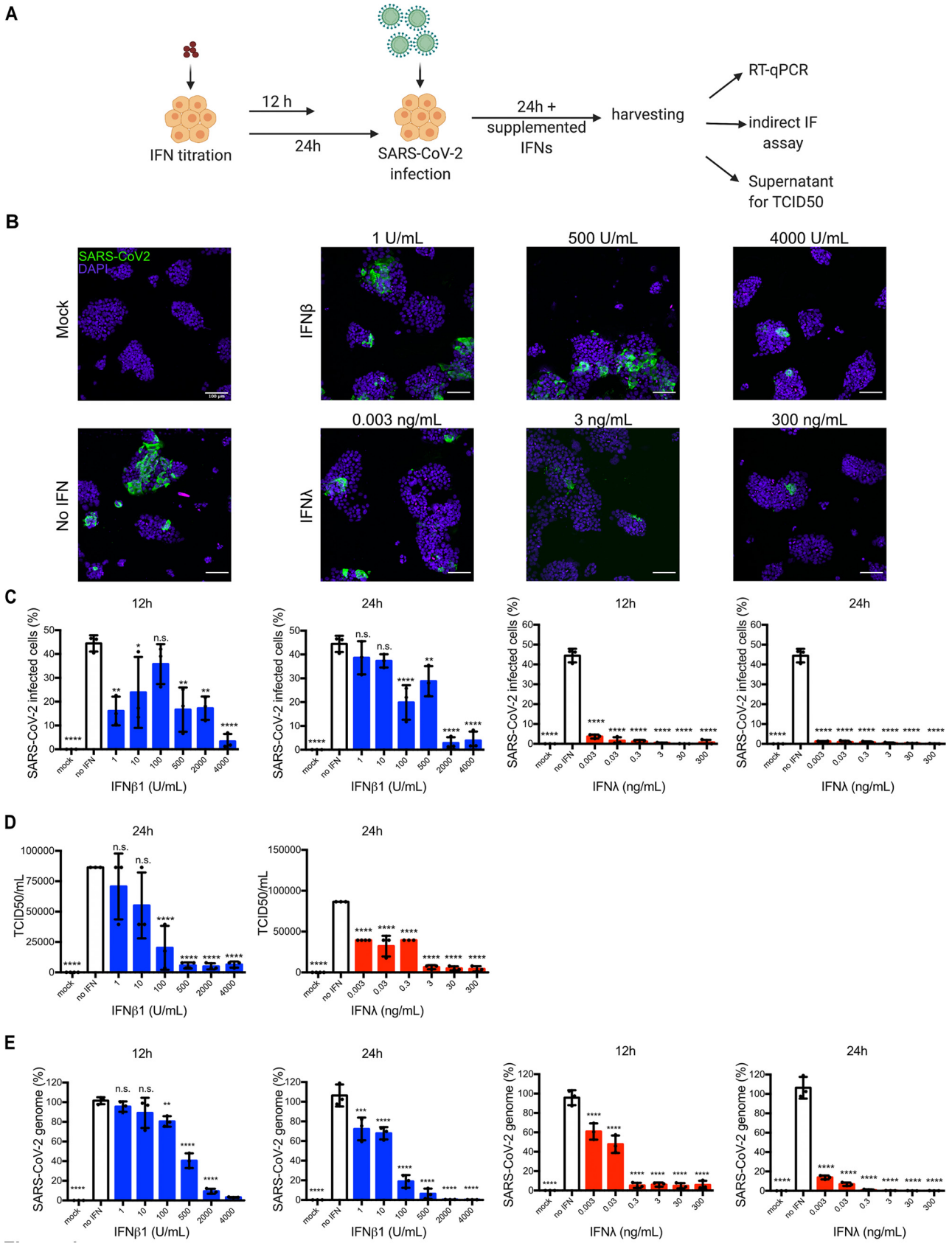

FIG 4 Exogenously added type I and III IFNs inhibit SARS-CoV-2 infection of hIECs in a concentration-dependent manner. (A to E) WT T84 cells were mock treated or pretreated with increasing concentration of type I (IFN-β1) and type III (IFN-λ1/2/3) IFNs for 12 or 24 h prior to infection. Cells were

(Continued on next page)

At 24 hpi, the cells were analyzed for virus infection by immunofluorescence for the SARS-CoV-2 nucleoprotein, by qRT-PCR against the virus genome, and for the release of *de novo* infectious particles into the supernatant (Fig. 4A). Immunofluorescence staining revealed that both type I and type III IFNs could reduce SARS-CoV-2 infection in a dose-dependent manner (Fig. 4B and C), and quantification of the number of infected cells revealed that both IFNs significantly impaired SARS-CoV-2 infection in a dose- and time-dependent manner (Fig. 4C). Intriguingly, we noticed that for cells treated with low concentrations of type I IFNs for 12 h, we had a greater inhibition of SARS-CoV-2 infection compared to a larger amount of IFN. While the molecular reason for this inverted dose-dependent response (at low concentrations) is not known, one possibility is that at low IFN concentrations, an antiviral state can be induced while activation of the negative regulatory feedback loop of type I IFNs is poorly activated, resulting in a greater antiviral state compared to higher concentrations. Interestingly, high doses of type I IFN were necessary to reduce SARS-CoV-2 infection to 10% of the cells (>2,000 U/mL) (Fig. 4B and C). In contrast, type III IFNs were able to restrict virus infection even at the lowest concentration (0.003 ng/mL) to below 5% infected cells (Fig. 4C). Concomitantly, when addressing the release of infectious particles into the supernatants of 24-h-IFN-pretreated and SARS-CoV-2-infected T84 cells (Fig. 2A), we observed that IFN treatment significantly reduced the amount of newly produced virus confirming a correlation between IFN-dependent signaling activation and the inhibition of *de novo* virus production (Fig. 4D).

Similar to the observed reduction in the number of SARS-CoV-2-infected cells and release of infectious particles upon IFN treatment (Fig. 4C and D), both type I and type III IFNs lead to a dose-and time-dependent decrease in viral replication, as monitored by evaluating the relative increase of SARS-CoV-2 N protein genome copy number over 24 h of infection (Fig. 4E). Likewise, quantitative measurement of ORF1a (Fig. 5A) and of the subgenomic virus RNA (Fig. 5B) through qRT-PCR also showed a concentration-dependent decrease in transcript copy number. Altogether, these results show that exogenous addition of IFNs prior to SARS-CoV-2 infection interferes with virus infection, replication, and the production of *de novo* infectious virus particles.

Taking into account that the units of measurement for type I and III IFNs are not comparable since IFN-β1 is expressed as antiviral activity (U/mL), while IFN-λ1/2/3 is expressed as weight (ng/mL), we were further interested to determine whether these low type III IFN concentrations were acting with the same efficiency on other viruses. Vesicular stomatitis virus (VSV) is often used as a gold standard in virology to study the effect of IFN on viral infection (reviewed in reference 45); therefore, we performed the same pretreatment experiment using different IFN concentrations as for SARS-CoV-2 (Fig. 4A) but with VSV expressing luciferase (VSV-Luc). T84 WT cells were pretreated with either IFN, as before, for 12 or 24 h and then infected with VSV-Luc. At 8 hpi, a luciferase assay was performed to determine virus infection levels (Fig. 6A). Interestingly, 0.003 and 0.03 ng/mL of type III IFN were not enough to significantly inhibit VSV-Luc infection (Fig. 6C), whereas low concentrations of type III IFNs were efficient against SARS-CoV-2 even with only 12 h of pretreatment (Fig. 4C and E). In contrast, type I IFN appears to have a slightly better antiviral activity on VSV compared to SARS-CoV-2 (Fig. 6B and Fig. 4C). Comparing the antiviral activities of type I and type III IFNs on VSV and SARS-CoV-2 highlights the potential sensitivity of SARS-CoV-2 to type III IFNs.

Interestingly, when comparing the effects on type I and III IFN pretreatments on both the number of SARS-CoV-2-infected cells and genome replication, we could observe that

FIG 4 Legend (Continued)
infected with SARS-CoV-2 using an MOI of 0.04 (as determined in Vero cells). At 24 hpi, the cells were harvested to assay virus infection and replication. (A) Schematic of infection conditions. (B) Cells were fixed, and indirect immunofluorescence analysis was performed against the viral nucleocapsid (green). Nuclei were stained with DAPI (blue). Representative images are shown. Scale bars, 100 μm. (C) The percentage of SARS-CoV-2-positive cells was quantified from the images in panel B. (D) Supernatants of 24-h-IFN-pretreated and infected WT T84 cells were harvested and titrated on Vero cells. After 24 h, the Vero cells were fixed, and the $TCID_{50}$/mL of newly produced particles was determined by in-cell Western blotting with an antibody against the viral nucleocapsid. The data are expressed as percentages, setting non-IFN-treated cells to 100%. (E) RNA was harvested, and qRT-PCR was used to evaluate the replication of the SARS-CoV-2 genome using primers that target nucleocapsid transcript. The data are normalized to input and expressed as percentages, setting non-IFN-treated cells to 100%. In panels C to E, the error bars indicate the standard deviations (n = 3 biological replicates). n.s., not significant; *, $P < 0.05$; **, $P < 0.01$; ***, $P < 0.001$; ****, $P < 0.0001$ (as determined by an ordinary one-way ANOVA with Dunnett's multiple-comparison test using nontreated infected cells as a reference).

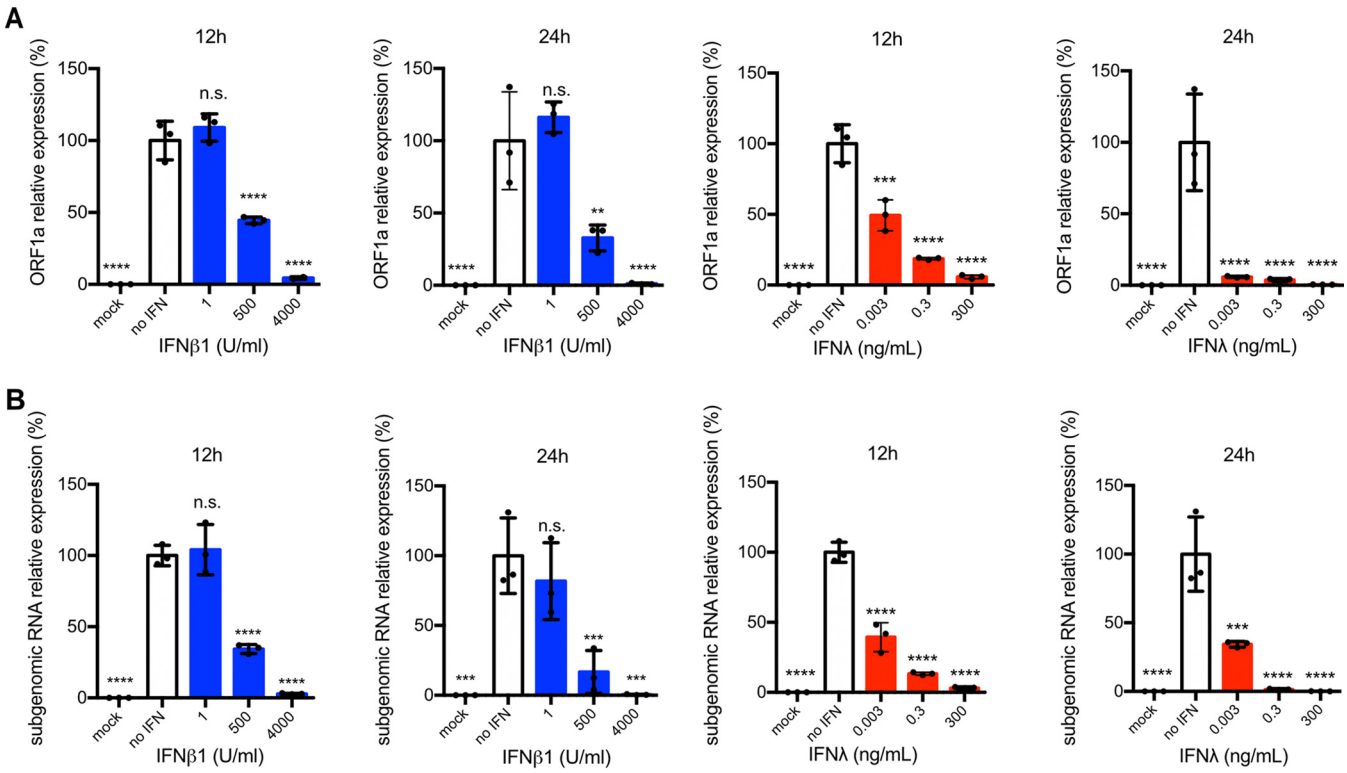

FIG 5 Exogenously added IFNs inhibit virus transcript levels in a concentration-dependent manner. (A and B) WT T84 cells were mock treated or pretreated with increasing concentration of type I (IFN-β1) and type III (IFN-λ1/2/3) IFNs for 12 and 24 h prior to infection. The cells were infected with SARS-CoV-2 using an MOI of 0.04. At 24 hpi, the cells were harvested to assay virus infection and replication. The RNA was harvested, and qRT-PCR was used to evaluate SARS-CoV-2 replication using primers that target ORF1a transcripts (A) and viral subgenomic RNA (B). The data are normalized to input and expressed as percentages, setting non-IFN-treated cells to 100%. Error bars indicate the standard deviations (n = 3 biological replicates). n.s., not significant; **, $P < 0.01$; ***, $P < 0.001$; ****, $P < 0.0001$ (as determined by ordinary one-way ANOVA with Dunnett's multiple-comparison test using nontreated infected cells as a reference).

longer IFN pretreatment and higher IFN concentrations were required to significantly reduce the SARS-CoV-2 genome copy number compared to the concentrations and time of pretreatment required to reduce the number of infected cells (Fig. 4C and E; Fig. 5). Such differences were especially significant for lower concentrations of IFN-treated cells for both IFN-β1 and IFN-λ1/2/3. To shed light on these differences, we treated T84 WT cells with either 1 U/mL of IFN-β1 or 0.003 ng/mL of IFN-λ1/2/3 for 12 h prior to SARS-CoV-2 infection and compared them to the nontreated virus-infected cells (Fig. 7A). Cells were harvested 24 hpi and immunostained with an antibody against the SARS-CoV-2 nucleoprotein or against double-stranded RNA (J2) to monitor nucleoprotein expression and viral genome replication, respectively (Fig. 7B). This allowed us to address whether there are discrepancies in virus genome replication and nucleocapsid translation at the single cell level. Quantification revealed that IFN mock-treated cells showed a similar number of nucleocapsid-positive cells and J2-positive cells (Fig. 7B and C). Upon IFN treatment, the percentage of J2-positive cells did not change; however, the percentage of nucleocapsid-positive cells decreased (Fig. 7C). Interestingly, this decrease in the number of nucleocapsid-positive cells was more pronounced for the IFN-λ1/2/3-treated cells (Fig. 7B and C).

Altogether, we observed that virus genome replication (assessed by both double-strand RNA staining and transcript levels of the genomic and subgenomic RNA), as well as translation, is affected by IFN pretreatment. Differences between type I and type III IFNs suggest that the type III IFN is more effective in preventing SARS-CoV-2 protein translation than is type I IFN.

Pretreatment with type III IFNs mediates a faster antiviral response against SARS-CoV-2 than pretreatment with type I IFNs. To determine whether both type I and III IFNs require the same time to achieve a similar antiviral protection against SARS-CoV-2 in hIECs, we performed a time-course experiment to determine the time required for each IFN to induce an antiviral state. WT T84 cells were pretreated with either type I or type III IFN at

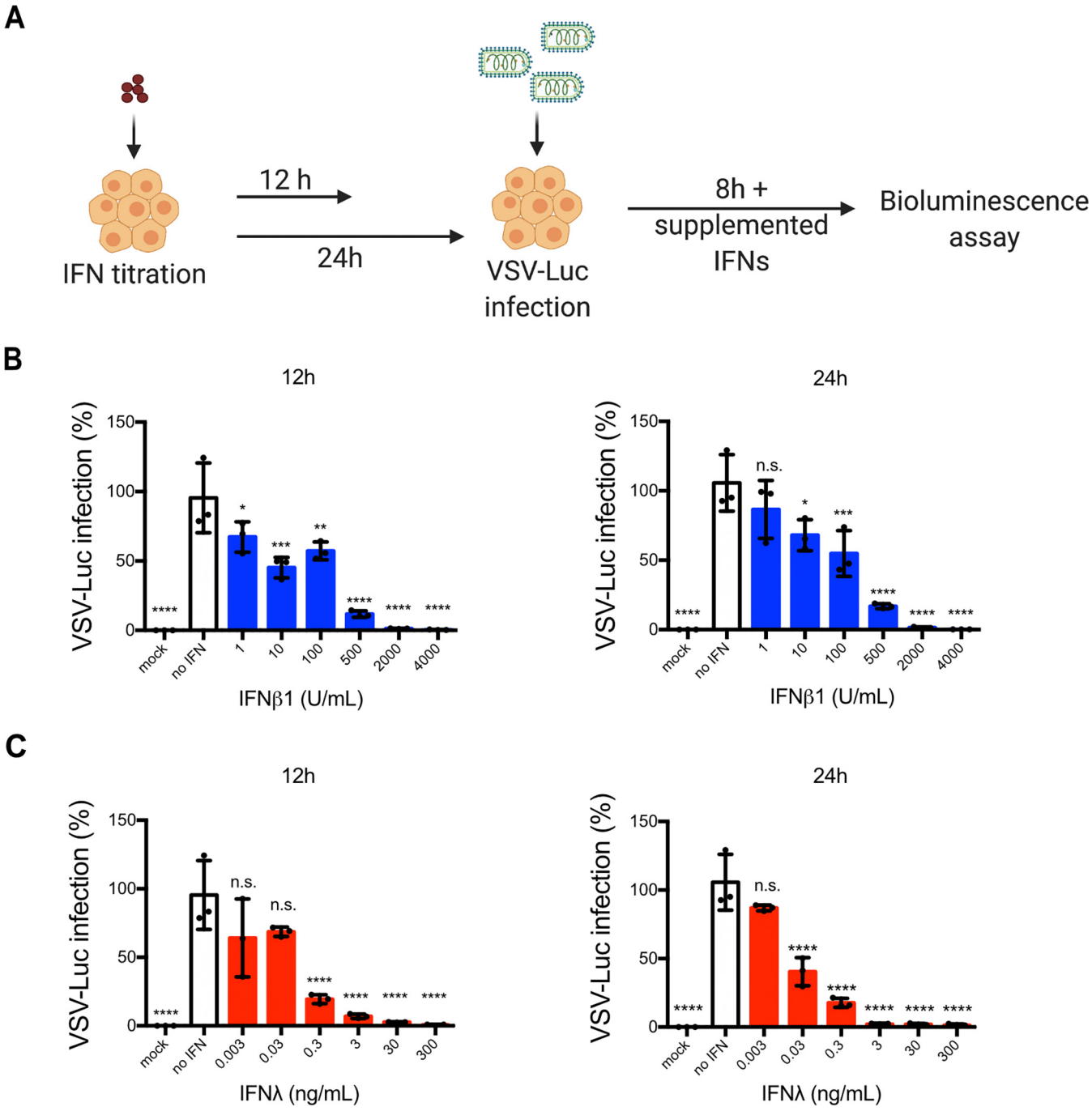

FIG 6 Exogenously added type I and III IFNs inhibit VSV-Luc infection of hIECs in a concentration-dependent manner. (A) Schematic of infection conditions. (B and C) WT T84 cells were mock treated or pretreated with increasing concentrations of type I (IFN-β1) (B) and type III (IFN-λ1/2/3) (C) IFNs for 12 and 24 h prior to infection. The cells were infected with VSV-Luc using an MOI of 5 (as determined in T84 wild type). At 8 hpi, the cells were harvested to assay virus infection with a luciferase assay. The VSV-Luc infection was quantified, and the results are expressed as percentages, setting non-IFN-treated cells to 100%. Error bars indicate the standard deviations (n = 3 biological replicates). n.s., not significant; *, $P < 0.05$; **, $P < 0.01$; ***, $P < 0.001$; ****, $P < 0.0001$ (as determined by ordinary one-way ANOVA with Dunnett's multiple-comparison test using nontreated infected cells as a reference).

different time points ranging from 24 to 3 h prior to infection with SARS-CoV-2. IFNs were maintained throughout the time course of virus infection and viral genome load, and the number of virus-infected cells was determined by qRT-PCR and immunofluorescence assay, respectively (Fig. 8A). 4000 IU/mL of IFN-β1 and 3 ng/mL of IFN-λ1-3 were evaluated as they led to complete inhibition of virus replication at 24h (Fig. 4). The results show that both type I and type III IFNs display similar kinetics of antiviral activity when using high

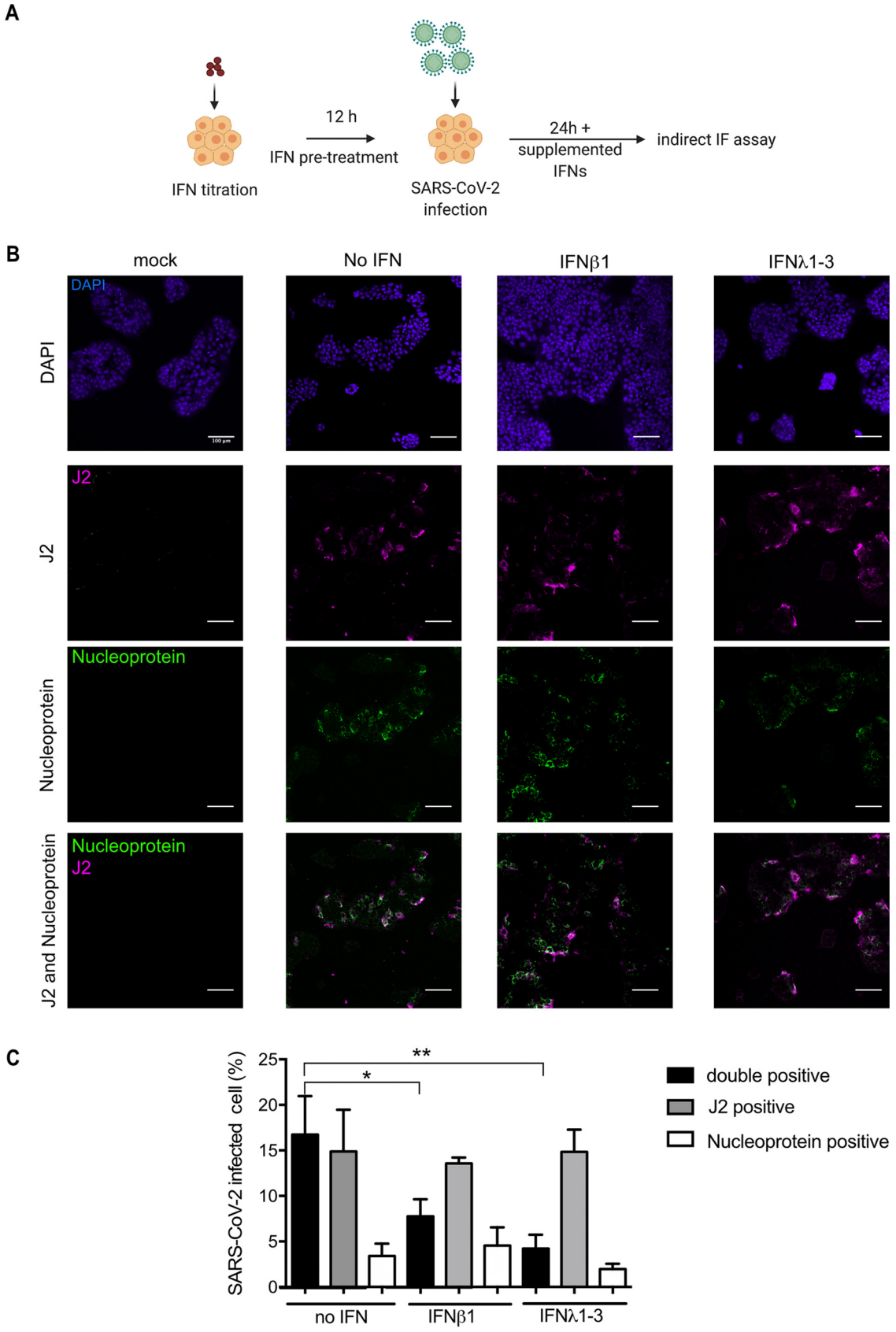

FIG 7 Type I and type III IFNs induce an antiviral state to protect against SARS-CoV-2 in hIECs by interfering with nucleocapsid expression. (A to C) WT T84 cells were mock treated or pretreated with type I and III IFN at low concentrations (1 U/mL IFN-β1 or

(Continued on next page)

concentrations of either IFN (Fig. 8B). Treating cells with either IFN for 3 h was sufficient to completely deplete SARS-CoV-2 infection, as determined by nucleocapsid immunostaining (Fig. 8B, left panels). The amount of viral genome was also greatly reduced by a 3-h pretreatment with either IFN, although only by around 60% compared to non-IFN-treated cells (Fig. 8B, right panels). Moreover, even at long IFN pretreatment times, during which no infected cells were detected by SARS-CoV-2 nucleocapsid immunostaining, the viral genome could still be detected (Fig. 8B).

Since the high IFN-concentrations were able to completely eliminate virus infection, we next addressed whether a lower concentration of type I or type III IFNs would impact the kinetics of the antiviral program against SARS-CoV-2. We chose to use a concentration of IFNs that led to a 50% reduction in genome replication (Fig. 4E). T84 WT cells were pretreated with 500 U/mL of IFN-β1 or 0.03 ng/mL of IFN-λ1/2/3 for different times prior to infection with SARS-CoV-2 (Fig. 8A). The results show that a 24-h pretreatment with a low concentration of type I IFN is required to significantly reduce the numbers of SARS-CoV-2-infected cells and viral genome copies (Fig. 8C). Shorter incubation times with type I IFNs does not lead to any decrease in the number of infected cells or the amount of virus genome copies (Fig. 8C). In contrast, shorter treatment times with type III IFNs led to a decrease in the numbers of infected cells and the amounts of virus genome copies (Fig. 8C). Furthermore, a 24-h pretreatment with 0.03 ng/mL of IFN-λ1/2/3 completely depleted the number of SARS-CoV-2 cells that are positive for nucleocapsid protein and significantly reduced the number of virus genome copies (Fig. 8C). These results strongly suggest that type III IFN requires less time to establish an antiviral effect against SARS-CoV-2 compared to type I IFNs.

This faster kinetics of antiviral protection of type III IFNs is interesting since previous work has shown that type III IFNs require a longer time to establish their antiviral state (29, 46–50). To determine whether the fast type III IFN-induced antiviral effect against SARS-CoV-2 infection is virus specific, we used both high and low IFN concentrations and conducted the same time-course experiment on T84 WT cells infected with VSV-Luc (Fig. 8A). Similar to previous work, an 8-h pretreatment with type I IFN at high concentrations was sufficient to reduce VSV infection by 90%, whereas type III IFN required 24 h to achieve a 90% reduction in infectivity (Fig. 8D). In addition, experiments performed using low IFN concentrations further supported that type I IFNs can control VSV infection faster than type III IFNs (Fig. 8E). As such, a 24-h pretreatment with type III IFNs reduced VSV-Luc infection only by 30% compared to nontreated infected cells (Fig. 8E). These results confirm that low concentrations of type III IFN require more time to establish an antiviral state to inhibit VSV-Luc infection compared to type I IFNs. Finally, when we compared the antiviral activities of low concentrations for both type I and type III IFNs against SARS-CoV-2 and VSV (see Fig. 8C versus Fig. 8E), we observed that SARS-CoV-2 is more resistant to type I IFN compared to VSV and, most importantly, more sensitive to type III IFNs compared to VSV.

Altogether, these results suggest that type I IFNs require more time to establish an antiviral state in hIECs to control SARS-CoV-2 infection than do type III IFNs. Interestingly, the potency and time dependency of the IFN-induced antiviral state appears to also be virus specific, with SARS-CoV-2 being particularly sensitive to type III IFNs.

IFN pre- and posttreatment offers protection against SARS-CoV-2 spread. We have established that type III IFNs induce a better antiviral protection against SARS-CoV-2 compared to type I IFN when cells are treated prior to infection. To address whether IFNs can also exercise their antiviral activities after viral infection, T84 WT cells were infected with SARS-CoV-2 at an MOI of 0.04 (as determined in Vero cells) and treated at different time

FIG 7 Legend (Continued)
0.003 ng/mL IFN-λ1/2/3) at 12 h prior to infection with SARS-CoV-2 using an MOI of 0.04 (as determined in Vero cells). The cells were harvested at 24 h after SARS-CoV-2 infection. (A) Schematic of infection setup. (B) Cells were fixed, indirect immunofluorescence was performed against the viral nucleocapsid protein (green) and dsRNA (J2) (magenta), and nuclei were stained with DAPI (blue). Representative images are shown. Scale bar, 100 μm. (C) The percentages of both nucleocapsid-positive and J2-positive cells (double-positive cells) and J2-positive-only cells were quantified from panel B. Error bars indicate the standard deviations (n = 3 biological replicates). *, $P < 0.5'$ **, $P < 0.01$ (as determined by ordinary one-way ANOVA with Dunnett's multiple-comparison test to the nontreated infected cells as a reference).

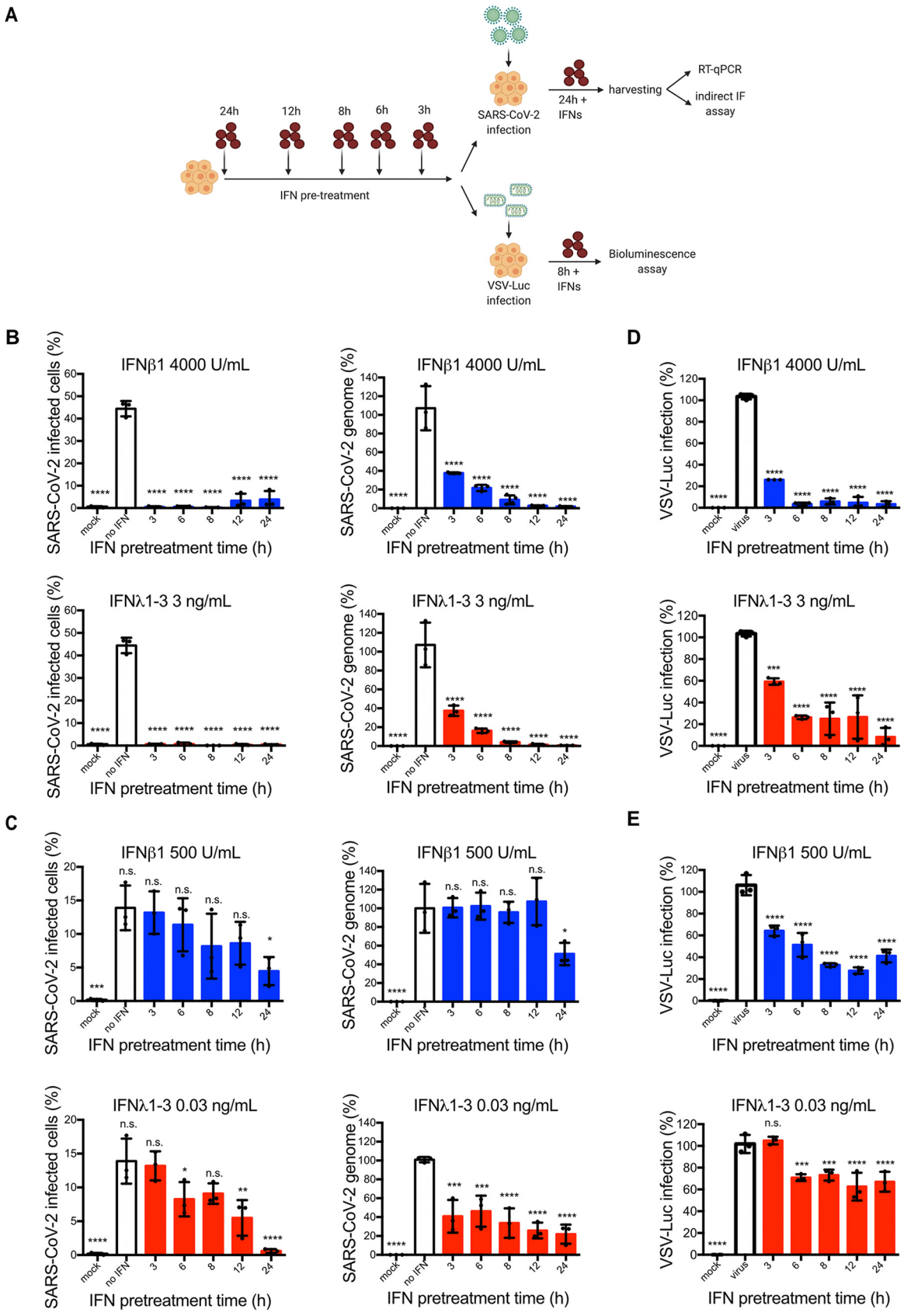

FIG 8 Differences between type I and type III IFNs in providing antiviral protection in hIECs against SARS-CoV-2 and VSV. (A to E) WT T84 cells were mock treated or pretreated with type I and III IFN at high (4,000 U/mL IFN-β1 or 3 ng/mL IFN-λ1/2/3) or low (500 U/mL

(Continued on next page)

points postinfection with either 4,000 U/mL of IFN-β1 or 3 ng/mL of IFN-λ1/2/3 (Fig. 9A). At 24 hpi, the virus genome copy number was evaluated, and the results show that both type I and III IFNs were able to inhibit viral replication when added up to 4 h postinfection; for type I IFN, the inhibition was visible even when adding up to 8 h postinfection (Fig. 9B). This effect was even stronger for *de novo* virus production. Even when we added type I IFNs at 8 hpi, no infectious viral particles could be detected in the supernatants of infected cells. Similarly, treating the cells with type III IFNs at 8 hpi led to a significant 15-fold reduction in particle release compared to nontreated cells (Fig. 9C). The discrepancies between virus genome copies and release of viral particles can be explained by the different sensitivities of the two assays used (qRT-PCR for genome copies and supernatant titration on Vero cells for infectious particle assessment). To validate the findings in nontransformed human intestinal epithelial cells, we exploited primary human ileum organoids. Organoids were seeded in two dimensions and infected with SARS-CoV-2 at an MOI of 0.04 (as determined in Vero cells) and treated with IFNs at different times postinfection (Fig. 9D). Similar to the colon carcinoma-derived T84 cells, virus replication (Fig. 9E) and *de novo* virus release (Fig. 9F) was significantly impaired by posttreatment with type I and III IFNs in ileum organoids.

To determine how long the IFN-mediated antiviral state persists, T84 WT cells were treated with either 4,000 U/mL of IFN-β1 or 3 ng/mL of IFN-λ1/2/3 for 24 h; the cells were then washed, and fresh medium lacking IFNs was added. At 12, 24, 48, or 72 h after medium exchange, WT T84 cells were infected with SARS-CoV-2 at an MOI of 0.04 (as determined in Vero cells) (Fig. 10A). At 8 hpi, the virus genome copy number was determined via qRT-PCR, and the results showed that the antiviral state induced by both type I and III IFNs persisted for up to 72 h (Fig. 10B). Interestingly, protection induced by type I IFN strongly decreased over time; by 12 h after medium exchange of IFN-β1-treated cells the infection levels were reduced by 90%, by 48 h after medium exchange the infection was reduced to 50%, and by 72 h after medium exchange the antiviral effect was almost lost (Fig. 10B). IN contrast, type III IFNs induce a longer-lasting and more potent antiviral state. Even at 48 h after medium exchange, virus replication was decreased by 75%, and the antiviral effect was still present 72 h after reducing the virus burden by 50% compared to non-IFN-treated cells (Fig. 10B). In parallel, at 24 hpi, the supernatants of infected WT T84 cells were titrated on Vero cells to determine the release of infectious viral particles with or without treatment. In accordance with viral replication levels (Fig. 10B), the release of infectious viral particles was also controlled more strongly upon treatment with type III IFNs compared to type I IFNs in WT T84 cells (Fig. 10C). For type III IFN treatment, release of infectious particles was reduced by 95% at 24 h after medium exchange and by 50% at 72 h after medium exchange compared to non-IFN-treated WT T84 cells (Fig. 10C). In contrast, no significant reduction in viral particles in the supernatant could be detected at 72 h after medium exchange when type I IFN treatment was performed (Fig. 10C).

The persistence of the antiviral state induced by type I and III IFNs was also assessed in human ileum-derived organoids. Organoids were treated with IFNs for 24 h and, at 24, 48, and 72 h after medium exchange, the organoids were infected with SARS-CoV-2 at an MOI of 0.04 (as determined in Vero cells) (Fig. 10A). Similar to our colon carcinoma-derived T84 cells, both type I and III IFNs induced a lasting antiviral effect that was significant even 48 h after medium exchange compared to non-IFN-treated organoids (Fig. 10D and E). Interestingly, at 72 h after medium exchange, only type III IFN pretreatment was still able to reduce the viral

FIG 8 Legend (Continued)
IFN-β1 or 0.03 ng/mL IFN-λ1/2/3) concentrations for different time points prior to infection. The cells were infected with either SARS-CoV-2 at an MOI of 0.04 (as determined in Vero cells) or vesicular stomatitis virus expression firefly luciferase (VSV-Luc) at an MOI of 5 (as determined in wild-type T84 cells). At 24 hpi (SARS-CoV-2) or 8 hpi (VSV-Luc), the cells were harvested to assay virus infection. (A) Schematic of infection setup. (B and C) The percentages of SARS-CoV-2-positive cells were quantified by immunofluorescence (left panels), and viral replication was assessed by qRT-PCR (right panels). qRT-PCR data are normalized to input and expressed as percentages, setting non-IFN-treated cells to 100%. (D and E) VSV-Luc infection was assayed by measuring the luciferase activity at 8 hpi. The luciferase activities for IFN-treated samples were normalized to the luciferase activity of the mock-treated sample, which corresponds to 100%. (B to E) Error bars indicate standard deviations (n = 3 biological replicates). n.s., not significant; *, $P < 0.5$; **, $P < 0.01$; ***, $P < 0.001$; ****, $P < 0.0001$ (as determined by ordinary one-way ANOVA with Dunnett's multiple-comparison test using nontreated infected cells as a reference).

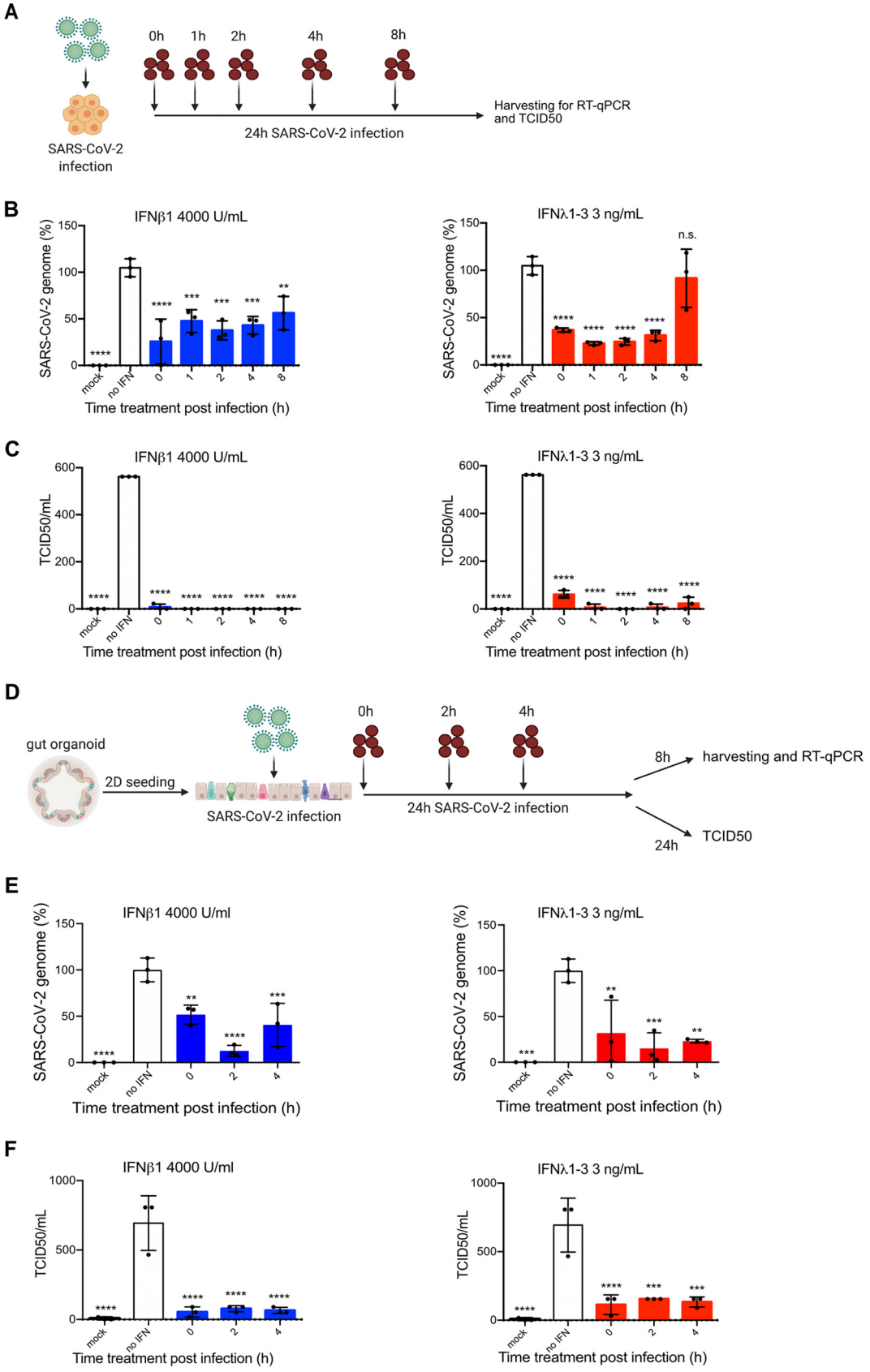

FIG 9 Kinetics of type I and III IFNs establishment of an antiviral state against SARS-CoV-2 in hIECs. (A to F) WT T84 cells or ileum-derived organoids were infected with SARS-CoV-2 at an MOI of 0.04 (as determined in Vero cells). At 0, 1, 2, 4, or 8 hpi,

(Continued on next page)

genome load by half compared to non-IFN-treated organoids (Fig. 10D). Moreover, at 48 and 72 h after medium exchange, type III IFNs restricted *de novo* particles in the supernatant better than did type I IFNs (Fig. 10E). Even at 72 h after medium exchange, treatment with type III IFNs significantly reduced the release of viral particles by more than 50% compared to non-IFN-treated organoids (Fig. 10E). In contrast, type I IFN treatment did not have a significant effect at 72 h after medium exchange compared to non-IFN-treated organoids (Fig. 10E). Together, these findings show that the type III IFNs can provide an antiviral state against SARS-CoV-2 infection which lasts longer compared to the protection provided by type I IFN treatment.

To address whether the long-term antiviral effect observed in hIECs was SARS-CoV-2 specific, T84 WT cells were infected with VSV-Luc after IFN washout (Fig. 10F). Interestingly, the antiviral state that both type I and III IFNs induced in WT T84 cells to restrict this virus was less pronounced compared to SARS-CoV-2 (Fig. 10G). Importantly, the protection against VSV-Luc induced by type I IFNs was longer lasting than for type III IFNs and reduced VSV-Luc infection significantly compared to no IFN treatment even 24 h after medium change (Fig. 10G). In contrast, for no time point after medium exchange was the type III IFN-induced antiviral state potent enough to significantly reduce VSV-Luc infection in hIECs (Fig. 10G), supporting the fact that the SARS-CoV-2 sensitivity to type III IFNs is virus specific.

Taken together, both IFNs are fast acting and can prevent viral replication and spread even when added after SARS-CoV-2 infection took place. Furthermore, our data suggest that type I and III IFNs can induce an antiviral state that lasts for several days. Type III IFNs are especially potent and long lasting since they can inhibit SARS-CoV-2 more efficiently compared to type I IFN.

DISCUSSION

There is increasing evidence that SARS-CoV-2 infection is not restricted to the respiratory tract but also impacts other organs (51) since viral components, such as RNA and proteins, were detected in patient biopsy specimens or in postmortem tissues such as the heart (52, 53), kidney (54), brain (54–56), and more. The gastrointestinal tract is one such important secondary organ, and a great fraction of COVID-19 patients display gastrointestinal symptoms and shed viral genomes within their feces (3, 5–13). This highlights the importance of understanding the molecular interaction of this specific virus with the gastrointestinal tract in order to better characterize and treat the associated pathogenesis and to curb the pandemic efficiently. Together, our results have shown that both type I and type III IFNs are efficient in mounting an antiviral immune response against SARS-CoV-2 in human intestinal epithelial cells, as seen by the rapid virus replication, *de novo* viral particle production, and spread in the absence of either type I or type III IFN receptors (Fig. 2). These observations highlight the significance of type I and type III IFN signaling during SARS-CoV-2 infection in the human intestinal epithelium, as opposed to murine models of SARS-CoV-2 infection, where type I IFN only minimally restricts SARS-CoV-2 (57). The importance of both IFNs in controlling SARS-CoV-2 in human tissue has been supported by several other studies (15, 17, 18, 31); however, the differences between the two types of IFNs have yet to be explored. Our results point out that there are indeed differences in the kinetics of antiviral properties of type I and III IFNs against SARS-CoV-2 infections in human intestinal epithelial cells. This, however, remains unclear in human lung epithelium since there are contradictory observations as to whether there is production of type I and III IFNs in the cells during SARS-CoV-2 infection (33–38). To the best of our knowledge, type III IFNs have been vastly neglected,

FIG 9 Legend (Continued)
4,000 U/mL of IFN-β1 or 3 ng/mL of IFN-λ1/2/3 was added. (A and D) Schematic of experiment setup for WT T84 cells (A) and organoids (D). (B and E) At 24 hpi, RNA was harvested from WT T84 (B) and ileum-derived organoids (E) to assess virus replication levels using qRT-PCR. Data are normalized to the input and expressed as percentages, setting non-IFN-treated cells to 100%. (C and F) At 24 hpi, WT T84 (C) and ileum-derived organoid (F) supernatants were harvested and titrated on Vero cells. After 24 h, Vero cells were fixed, and the $TCID_{50}$/mL of newly produced particles was determined by in-cell Western blotting with an antibody against the viral nucleocapsid. (B, C, E, and F) Error bars indicate the standard deviations ($n = 3$ biological replicates). n.s., not significant; *, $P < 0.5$; **, $P < 0.01$; ***, $P < 0.001$; ****, $P < 0.0001$ (as determined by ordinary one-way ANOVA with Dunnett's multiple-comparison test using nontreated infected cells as a reference).

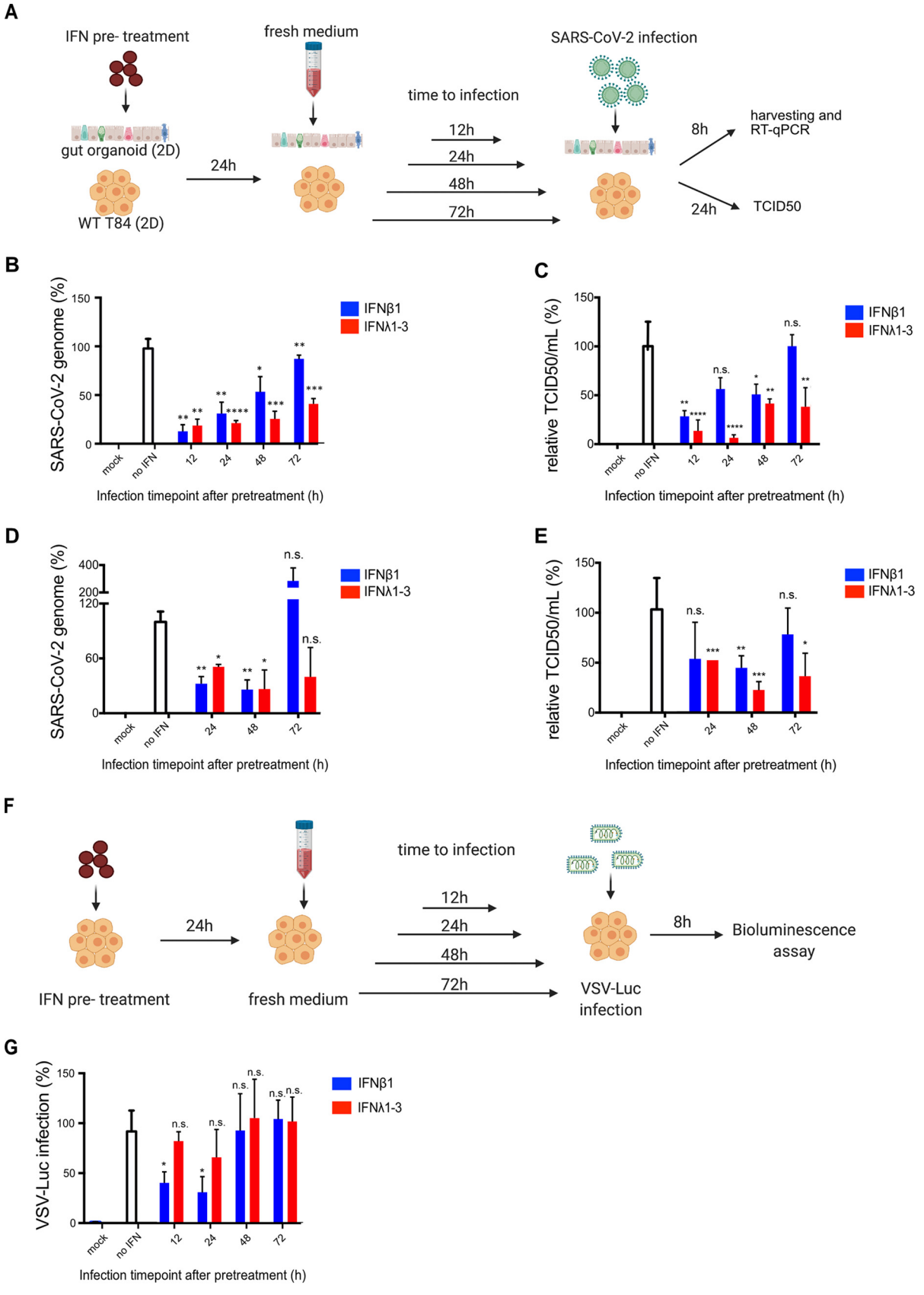

FIG 10 Type III IFNs induce a longer lasting antiviral state in hIECs against SARS-CoV-2 infection compared to type I IFN. (A to G) WT T84 cells or ileum-derived organoids were mock treated or pretreated with 4,000 U/mL of IFN-β1 or 3 ng/mL of IFN-λ1/2/3. At 24 h after

(Continued on next page)

although some studies showed that the human lung epithelium is also sensitive to type III IFN treatment (38, 40, 43). Importantly, no similar direct comparison of the antiviral activities of both type I and type III IFNs has been performed in human lung epithelial cells. Interestingly, inhibition of *de novo* infectious virus production in Calu-3 cells suggests that type I IFN would be more potent than type III IFNs (40). This further highlights the importance of studying SARS-CoV-2 in multiple cellular models covering the broad tropism of SARS-CoV-2 since the sensitivity of this pathogen to various antiviral strategies might be organ specific.

We showed by immunostaining of the virus nucleocapsid protein and quantification of the viral genome that both type I and III IFNs restrict SARS-CoV-2 in a concentration-dependent manner (Fig. 4). Interestingly, inhibition of nucleocapsid protein with a certain IFN concentration did not mirror the inhibition of the virus genome, since the genome load was still measured in samples where no nucleocapsid could be detected. To analyze in more detail the discrepancy between the viral genome copy number and number of infected cells, we further determined whether infected and treated cells were positive for J2, which labels double-stranded RNA (dsRNA) and is representative for virus RNA synthesis and genome transcription and nucleocapsid protein representing the translation of structural proteins. We have shown that, in contrast to SARS-CoV-2-infected cells without treatment, having similar levels of viral dsRNA and nucleocapsid protein, IFN-treated cells can be positive for viral dsRNA, while no nucleocapsid protein could be detected (Fig. 7). This observation is especially prominent in type III IFN-treated cells. The results suggest that one putative mechanism of IFNs to restrict virus spread is by inhibiting virus translation of subgenomic RNA and thereby the expression of structural proteins. For example, immediately after entry, the genomic virus RNA undergoes a first step of translation of the ORF1a/b polyprotein, which results in nonstructural proteins that form the viral replication and transcription complex (58). That our results show virus RNA synthesis and subgenomic RNA transcripts in samples without N-protein expression suggests that the initial virus genome translation of nonstructural proteins is less affected by IFN treatment than the later translation of structural proteins. Previously, it was reported that type I IFN treatment during dengue virus and HIV infection can affect virus protein translation (59, 60). However, little is known about type I and especially type III IFN-mediated inhibition of coronavirus nucleocapsid translation, specifically for SARS-CoV-2-infection. Our observation suggests a possible mechanism on the mode of action of IFN-dependent signaling on SARS-CoV-2 and shows that type I and III IFNs efficiently restrict the spread of SARS-CoV-2 in human epithelium after virus entry by inhibiting the production of nucleocapsid (and probably other viral proteins) and thus reducing the release of functional virus particles to neighboring cells. More needs to be done to decipher the details of this mechanism underlying the IFN-mediated inhibition of viral genome replication and translation. Indeed, several ISGs were found to inhibit viral protein translation and might be good candidates as key cellular players in the IFN-dependent response to SARS-CoV-2. A well-investigated type I and III-induced ISG is PKR, which upon activation phosphorylates EIF2α to halt cellular translation (61). Also, the IFIT family was demonstrated to suppress cellular translation upon virus infections by several mechanisms (62, 63). Moreover, ISG20 was shown to impair translation of virus protein without affecting cellular protein translation by discriminating self from non-self (64).

Our data support that type I and type III IFNs induce a dose- and time-dependent inhibition of viral infection in hIECs. Interestingly, our results strongly suggest that type III IFNs were able to restrict virus infection at a lower dosage and with shorter treatment times

FIG 10 Legend (Continued)
treatment, fresh medium was added to the cells. At 12, 24, 48, or 72 h after medium exchange, the cells were infected with SARS-CoV-2 or VSV-Luc. (A and F) Schematic of experiment setup for SARS-CoV-2 infection (A) and VSV-Luc infection (F). (B and C) Infection with SARS-CoV-2 using an MOI of 0.04 (as determined in Vero cells). At 8 hpi, RNA was harvested to assess virus replication levels in WT T84 cells (B) and ileum-derived organoids (D) using qRT-PCR, and the virus genome was normalized to the input. At 24 hpi, supernatants of WT T84 cells (C) and ileum-derived organoids (E) were harvested and titrated on Vero cells. After 24 h, Vero cells were fixed, and the $TCID_{50}$/mL of newly produced particles was determined by in-cell Western blotting with an antibody against the viral nucleocapsid. (G) Infection with VSV-Luc using an MOI of 5 (as determined in the T84 wild type). At 8 hpi, a luciferase assay was performed to determine virus infection levels. (B, E, and G) SARS-CoV-2 genome copy number, $TCID_{50}$/mL of newly produced particles, and VSV-Luc infection levels were normalized to the nontreated infected cells at the respective time point. Error bars indicate the standard deviations ($n = 3$ biological replicates). n.s., not significant; *, $P < 0.5$; **, $P < 0.01$; ***, $P < 0.001$; ****, $P < 0.0001$ (as determined by a two-tailed unpaired t test with Welch's correlation, using nontreated infected cells for the respective time points as a reference).

compared to type I IFNs. Comparing whether type I or type III IFNs are more potent antiviral at the same concentrations is intrinsically difficult since the IFNs are available at concentrations expressed in different units. The type III IFNs are available in protein concentrations (ng/mL), while the type I IFN concentration is expressed as an antiviral activity (U/mL). Interestingly, our observations suggest that type III IFNs are more potent and faster acting on SARS-CoV-2, in contrast to a previous study using VSV infection of hIECs (29), which showed that type III IFNs need more time to confer protection. To address these discrepancies, we compared the effects of both type I and type III IFNs on VSV and SARS-CoV-2 infection (Fig. 6, 8, and 10). We could reproduce our previous results that type I IFN was more potent in inhibiting VSV infection, especially at lower concentrations. By comparing SARS-CoV-2 and VSV infections, we could show that low concentration of type I IFN was able to control VSV infection, while having little to no effect on SARS-CoV-2 infection (Fig. 4, 6B, and 8). Reciprocally, low concentrations of type III IFNs were able to control SARS-CoV-2, but with limited to no impact on VSV (Fig. 4 and 6C). These differences in the efficacy of type I and type III IFNs in providing, in the same cell type, antiviral protection against two distinct viruses suggest that two distinct antiviral states are achieved upon type I and type III IFN treatment and that these states are more potent against specific viruses. While there is very limited evidence that type I and type III IFN induce the expression of different ISGs (65), it recently became clear that both cytokines induce the same ISGs, but with very different kinetics, likely creating a distinct antiviral state (29, 32, 47, 66–69).

Lastly, we have demonstrated that the addition of IFNs after SARS-CoV-2 infection was still able to inhibit viral replication and *de novo* virus production not only in the hIEC WT T84 cell model but also in nontransformed human ileum-derived organoids (Fig. 9), an observation which further highlights the effectiveness of IFN treatments against SARS-CoV-2 infection. Importantly, we could show that type III IFNs were able to provide longer-lasting protection against SARS-CoV-2 compared to type I IFNs and that such potent antiviral states persist and are able to inhibit virus replication for more than 72 h upon withdrawal (Fig. 10B to E). This effect is specific for SARS-CoV-2, since no such long-lasting effect was determined upon VSV-Luc infection (Fig. 10F and G). Altogether, we see that type III IFNs act fast, require low concentrations and short pretreatment times, and offer long-lasting antiviral protection against SARS-CoV-2 in hIECs. These observations suggest type III IFN treatment as a strong therapeutic candidate against SARS-CoV-2 infection of the human intestine.

The use of IFN-β alone or in combination with other antiviral agents to treat SARS-CoV-1 infection has been suggested (70). Furthermore, clinical trials using treatment combining intravenous injection of IFN-β1 and lopinavir/ritonavir were performed in Saudi Arabia to treat MERS-CoV (71, 72). IFN-β1 seems to be the most efficient IFN to curb coronavirus infection, and a report shows that this is due to the fact that IFN-β1 can induce the production of adenosine with anti-inflammatory properties and maintain endothelial barrier function in pulmonary endothelial cells via upregulation of cluster of differentiation 73 (CD73) (73). SARS-CoV-2 is thought to be more sensitive to IFN treatment due to its truncated Orf6 and Orf3 proteins, as opposed to those of SARS-CoV-1 and MERS-CoV, due to a loss of their inhibitory effects on the IFN signaling pathway (40, 74). There is currently a treatment consisting of a triple combination of IFN-β1b, lopinavir/ritonavir, and ribavirin to treat patients with COVID-19 in Hong Kong as a phase-2 trial (75). This trial has yielded promising outcomes showing symptom alleviation and a reduction in viral shedding duration in patients with mild to moderate COVID-19 disease in the hospital (75). Another study also pointed out that IFN-β-1a, when administered at clinically permissible concentration after SARS-CoV-2 infection, was highly effective at inhibiting *in vitro* SARS-CoV-2 replication (76).

Here, we have demonstrated that, compared to type I IFNs, type III IFNs are more potent in protecting human intestinal epithelial cells against SARS-CoV-2. This suggests type III IFNs might offer a promising option for treating SARS-CoV-2 infection, particularly in the context of the human intestinal epithelium. Given the lower dose and shorter treatment required to confer an antiviral state, as well as the fact that type III IFN antiviral activity persists longer than type I IFN-mediated activity, it is likely that the administration of type III IFN to patients would be more beneficial and require a less-frequent regimen which will render

TABLE 1 Compounds and concentrations for human organoid basal and differentiation media[a]

Basal medium		Differentiation medium	
Compound	Final concn	Compound	Final concn
L-WRN	50% (by vol)	B27	1:50
B27	1:50	*N*-Acetylcysteine	1 mM
N-Acetylcysteine	1 mM	R-spondin	5% (by vol)
EGF	50 ng/mL	Noggin	50 ng/mL
A83-01	500 nM	EGF	50 ng/mL
IGF-1	100 ng/mL	Gastrin	10 mM
FGF basic	50 ng/mL	A83-01	500 nM
Gastrin	10 mM		

[a]The compound included Ad DMEM/F-12 + GlutaMAX + HEPES + penicillin/streptomycin.

this approach more amenable as therapeutic option. Importantly and as reviewed before (77), type I IFN treatment was shown to support development of autoimmune diseases and can induce tissue damage. We believe that type III IFNs could potentially be the superior choice of treatment than type I IFNs in treating SARS-CoV-2 in patients.

MATERIALS AND METHODS

Cell line and viruses. Wild-type T84 (ATCC CCL-248) and their IFN receptor knockouts (30) were cultured in a 50:50 mixture of Dulbecco modified Eagle medium (DMEM) and F-12 (Gibco) supplemented with 10% fetal bovine serum and 1% penicillin/streptomycin (Gibco). T84 WT and IFN receptor knockout cell lines carrying the H2B fluorescent nuclear tag were generated by lentiviral transduction and antibiotic selection. Vero E6 cells (ATCC CRL 1586) were cultured in DMEM (Gibco) supplemented with 10% fetal bovine serum and 1% penicillin/streptomycin (Gibco). IFN-α/β reporter HEK293 cells (Invivogen, catalog no. hkb-ifnab) and IFN-λ Reporter HEK293 Cells (Invivogen, catalog no. hkb-ifnl) were maintained in Iscove's modified Dulbecco medium (Gibco) supplemented with 10% fetal bovine serum and 1% penicillin/streptomycin (Gibco).

SARS-CoV-2 was isolated from an infected patient at the University Hospital Heidelberg. The virus was amplified in Vero E6 cells, and P3 virus stocks were used in all experiments (31). VSV-Luc was prepared and used as previously described (29).

Human organoid culture. Human tissue was received from ileum resection from the University Hospital Heidelberg. This study was carried out in accordance with the recommendations of the University Hospital Heidelberg with informed written consent from all subjects in accordance with the Declaration of Helsinki. All samples were received and maintained in an anonymized manner. The protocol was approved by the Ethics Commission of the University Hospital Heidelberg (protocol S-443/2017). Crypt-containing stem cells were isolated following dissociation of tissue sample in 2 mM EDTA for 1 h at 4°C. Crypts were spun and washed in ice-cold phosphate-buffered saline (PBS). Fractions enriched in crypts were filtered with 70 mM filters, and the fractions were observed under a light microscope. Fractions containing the highest number of crypts were pooled and spun again. The supernatant was removed, and crypts were resuspended in Matrigel. Crypts were passaged and maintained in basal and differentiation culture media (Table 1).

Organoids were seeded in two dimensions prior to treatment and infection. For this, 48-well plates were coated with rat collagen in ethanol for 2 h at 37°C prior to organoid seeding. Organoids were collected at a ratio of 100 organoids/well. Collected organoids were spun at 450 $\times$ *g* for 5 min, and the supernatant was removed. The organoids were washed 1$\times$ with cold PBS and spun at 450 $\times$ *g* for 5 min. The PBS was removed, and the organoids were digested with 0.05% trypsin-EDTA (Life Technologies) for 5 min at 37°C. Digestion was stopped by adding serum-containing medium. The organoids were spun at 450 $\times$ *g* for 5 min, the supernatant was removed, and the organoids were resuspended in basal medium at a ratio of 250 mL of medium/well. The collagen mixture was removed from the 48-well plate, and 250 mL of organoids was added to each well. For organoid differentiation, the medium was changed at 1 day postseeding to differentiation medium (see Table 1), and cells were kept in differentiation medium for at least 4 days. All of the following steps, including IFN-treatment and virus infection, were performed in differentiation media.

Viral infections. All SARS-CoV-2 infections were performed at an MOI of 0.04, as determined in Vero E6 cells. Prior to infection, the culture medium was removed, and virus was added to cells, followed by incubation for 1 h at 37°C. After the incubation, the virus was removed, and fresh medium or medium supplemented with the indicated IFNs was added back to the cells upon virus removal.

Interferon treatment. Human recombinant IFN-β was obtained from Biomol (catalog no. 86421). Recombinant human IFN-λ1 (IL-29; catalog no. 300-02L), IFN-λ2 (IL-28A; catalog no. 300-2K), and IFN-λ3 (IL-28B; catalog no. 300-2K) were purchased from Peprotech. The IFN concentrations used to treat the cells and the duration of the treatments are stated in the figure legends.

RNA isolation, cDNA synthesis, and qRT-PCR. Cells were harvested either 4, 8, 12, or 24 hpi, and RNA was isolated using an RNeasy RNA extraction kit (Qiagen) according to the manufacturer's instructions. cDNA was synthesized using iSCRIPT reverse transcriptase (Bio-Rad) from 250 ng of total RNA per 20-μL reaction according to the manufacturer's instructions. A qRT-PCR assay was performed using iTaq SYBR green (Bio-Rad) according to the manufacturer's instructions. The expression of target genes was normalized to the endogenous control *TBP*. The primer sequences are given in Table 2.

TABLE 2 Primer sequences used for qRT-PCR

		Sequence (5′–3′)	
Target gene	**Species**	**Forward**	**Reverse**
TBP	Human	CCACTCACAGACTCTCACAAC	CTGCGGTACAATCCCAGAACT
IFN-β1	Human	GCCGCATTGACCATCTAT	GTCTCATTCCAGCCAGTG
IFN-λ2/3	Human	GCCACATAGCCCAGTTCAAG	TGGGAGAGGATATGGTGCAG
IFIT1	Human	AAAAGCCCACATTTGAGGTG	GAAATTCCTGAAACCGACCA
Viperin	Human	GAGAGCCATTTCTTCAAGACC	CTATAATCCCTACACCACCTCC
SARS-CoV-2 N protein	SARS-CoV-2	GCCTCTTCTCGTTCCTCATCAC	AGCAGCATCACCGCCATT
SARS-CoV-2 ORF 1a	SARS-CoV-2	GAGAGCCTTGTCCCTGGTTT	AGTCTCCAAAGCCACGTACG
SARS-CoV-2 subgenomic RNA	SARS-CoV-2	TCCCAGGTAACAAACCAACCAACT	AAATGGTGAATTGCCCTCGT

SARS-CoV-2 N protein transcript levels were used to assess the virus genome copy number. SARS-CoV-2 orf1a and subgenomic RNA transcript levels were used for testing other aspects of the viral replication cycle. For all SARS-CoV-2 transcript levels, the fold change was calculated using the input as a reference. Input RNA was harvested immediately after a 1-h SARS-CoV-2 infection.

Western blot. Cells were harvested and lysed with 1× RIPA (150 mM sodium chloride, 1.0% Triton X-100, 0.5% sodium deoxycholate, 0.1% sodium dodecyl sulfate [SDS], 50 mM Tris [pH 8.0]) with phosphatase and protease inhibitors (Sigma-Aldrich) for 5 min at 37°C. Lysates were collected, and equal protein amounts were separated by SDS-PAGE and blotted onto a nitrocellulose membrane by wet blotting (Bio-Rad). Membranes were blocked with TBS-T containing 5% bovine serum albumin (BSA) for 2 h at room temperature. The primary antibodies beta-actin (Sigma #5441) and phospho-STAT1 (BD Transductions, catalog no. 612233) were diluted in the same blocking buffer, followed by incubation overnight at 4°C. Membranes were then washed three times with TBS-T for 10 min at room temperature with rocking. Anti-mouse antibodies coupled with horseradish peroxidase (HRP; GE Healthcare, catalog no. NA934V) were used at a 1:5,000 dilution in blocking buffer, followed by incubation at room temperature for 1 h with rocking. Membranes were washed three times with TBS-T for 10 min at room temperature with rocking. HRP detection reagent (GE Healthcare) was mixed 1:1, followed by incubation at room temperature for 5 min. Membranes were exposed to film and developed.

In-cell Western analyses ($TCID_{50}$). Vero E6 cells were seeded at 30,000 cells/well into a 96-well plate 24 h prior to infection. First, 100 μL of supernatant was added to the wells, and seven 1:5 serial dilutions were made. The cells were incubated for 24 h and then fixed with 2% paraformaldehyde (PFA) for 20 min at room temperature. Cells were washed twice with 1× PBS upon PFA removal and then permeabilized for 15 min with 0.5% Triton-X in PBS. Blocking was carried out with 1:2 dilution of Li-Cor blocking buffer in Tris-buffered saline for 30 min at room temperature. The cells were then incubated with a primary mouse monoclonal antibody against SARS-CoV-2 nucleocapsid protein (Sino Biologicals, catalog no. MM05; 1:1,000) for 1 h at room temperature. The cells were washed three times with PBS and then incubated with secondary antibody (anti-mouse CW800) and DNA dye Draq5 (Abcam) diluted 1:10,000 in blocking buffer for 1 h at room temperature. The cells were then washed again three times with PBS, and the plate was imaged on a LICOR (Li-Cor) imager.

Detection of IFNs in the supernatant by HEK-Blue assay. Supernatants of SARS-CoV-2-infected WT T84 cells were collected at 24 hpi. Virus in supernatants was inactivated with 0.05% beta-propiolactone (BPL; Sigma-Aldrich) overnight at 4°C. BPL was hydrolyzed at 37°C for 2 h prior to the HEK-blue assay. HEK-Blue assay standards were also diluted in 0.05% BPL overnight after 2 h of hydrolyzation at 37°C. IFN-α/β reporter HEK293 cells and IFN-λ reporter HEK293 cells were seeded in FBS-inactivated DMEM/F-12 medium at a density of 35,000 cells per well in 96-well plates 1 day before the experiment. Next, 50-μL portions of supernatants of SARS-CoV-2-infected WT T84 cells were added to HEK-Blue cells for 24 h, and the levels of secreted embryonic alkaline phosphatase was measured using QUANTI-Blue (InvivoGen, catalog no. rep-qbs). Since IFN-α/β reporter HEK293 cells are also able to respond to IFN-λ, cells were transfected with a previously generated CRISPR K.O vector targeting the IFNLR1 (29), generating a reporter cell line that can only sense type I IFNs.

Indirect immunofluorescence assay. Cells were seeded on iBIDI glass-bottom 8-well chamber slides previously coated with 2.5% human collagen in water. At the indicated times postinfection, the cells were fixed in 4% PFA for 20 min at room temperature. The cells were washed in 1× PBS, permeabilized in 0.5% Triton-X for 15 min, and blocked using 3% BSA-PBS for 30 min at room temperature. Mouse monoclonal antibody against SARS-CoV-2 nucleocapsid protein (Sino Biologicals, catalog no. MM05) was diluted in 1% BSA-PBS, followed by incubation for 1 h at room temperature. The cells were then washed with 1× PBS three times, followed by incubation with secondary antibodies conjugated with AF488 or AF647568 (Molecular Probes) and DAPI (4′,6′-diamidino-2-phenylindole) for 30 to 45 min at room temperature. Next, the cells were washed three times in 1× PBS and then maintained in PBS. The cells were imaged on a Nikon/Andor spinning disc confocal microscope to quantify the number of infected cells relative to the number of nuclei.

VSV luciferase assay. Wild-type T84 cells were seeded in a black F-bottom 96-well plate. The cells were treated as indicated in the text with type I or type III IFNs. VSV-Luc was added to the wells using an MOI of 5 as determined in wild-type T84 cells, and the infection was allowed to proceed for 8 h. At the end of the infection, the medium was removed, and the cells were washed 1× with PBS and lysed with cell lysis buffer (Promega) at room temperature for 20 min. A 1:1 dilution of Steady-Glo (Promega) and lysis buffer was added to the cells, followed by incubation at room temperature for 15 min. The luminescence was read using an Omega Luminometer.

Statistics and computational analyses and statistics. All statistical analysis was performed either by using ordinary one-way analysis of variance (ANOVA) Dunnett's multiple-comparison test or by using

a two-tailed unpaired *t* test with Welch's correlation (specified in the figure legends) with the GraphPad Prism software package.

In order to quantify infected cells from indirect immunofluorescence-stained samples, ilastik 1.2.0 was used on DAPI images to generate a mask representing each nucleus as an individual object. These masks were used on CellProfiler 3.1.9 to measure the intensity of the conjugated secondary antibodies in each nucleus. A threshold was set based on the basal fluorescence of noninfected samples, and all nuclei with a higher fluorescence were considered infected cells.

ACKNOWLEDGMENTS

This study was supported by research grants from Deutsche Forschungsgemeinschaft (DFG) projects 415089553 (Heisenberg program), 240245660 (SFB1129), and 272983813 (TRR179); from the state of Baden Wuerttemberg (AZ 33.7533.-6-21/5/1) and the Bundesministerium Bildung und Forschung (BMBF; 01KI20198A); and from within the ORGANOSTRAT funding program to S.B. M.L.S. was supported by the DFG (416072091) and the BMBF (01KI20239B). C.M.-Z. is supported by the SFB1129 (240245660). We also acknowledge funding from the Helmholtz International Graduate School for Cancer Research to C.K., the German Academic Exchange Service (DAAD; research grant 57440921) to P.D., and the China Scholarship Council and the Landesgraduirtenförderung (LGF) to C.G.

We thank Vibor Laketa and Sylvia Olberg from the Infectious Diseases Imaging platform for support with the imaging of infected cells.

C.M.-Z., C.K., and P.D. performed experiments, analyzed data, and helped with manuscript writing. C.G. performed the VSV experiments. S.B. and M.L.S. conceived experiments, interpreted results, and wrote the manuscript. The final version of the manuscript was approved by all authors.

We declare there are no competing interests.

REFERENCES

1. Lu H, Stratton CW, Tang YW. 2020. Outbreak of pneumonia of unknown etiology in Wuhan, China: the mystery and the miracle. J Med Virol 92:401–402. https://doi.org/10.1002/jmv.25678.
2. Haake C, Cook S, Pusterla N, Murphy B. 2020. Coronavirus infections in companion animals: virology, epidemiology, clinical, and pathologic features. Viruses 12:1023. https://doi.org/10.3390/v12091023.
3. Huang C, Wang Y, Li X, Ren L, Zhao J, Hu Y, Zhang L, Fan G, Xu J, Gu X, Cheng Z, Yu T, Xia J, Wei Y, Wu W, Xie X, Yin W, Li H, Liu M, Xiao Y, Gao H, Guo L, Xie J, Wang G, Jiang R, Gao Z, Jin Q, Wang J, Cao B. 2020. Clinical features of patients infected with 2019 novel coronavirus in Wuhan, China. Lancet 395:497–506. https://doi.org/10.1016/S0140-6736(20)30183-5.
4. Zhu N, Zhang D, Wang W, Li X, Yang B, Song J, Zhao X, Huang B, Shi W, Lu R, Niu P, Zhan F, Ma X, Wang D, Xu W, Wu G, Gao GF, Tan W, China Novel Coronavirus Investigating and Research Team. 2020. A novel coronavirus from patients with pneumonia in China, 2019. N Engl J Med 382:727–733. https://doi.org/10.1056/NEJMoa2001017.
5. Guan W, Ni Z, Hu Y, Liang W, Ou C, He J, Liu L, Shan H, Lei C, Hui DSC, Du B, Li L, Zeng G, Yuen K-Y, Chen R, Tang C, Wang T, Chen P, Xiang J, Li S, Wang J, Liang Z, Peng Y, Wei L, Liu Y, Hu Y, Peng P, Wang J, Liu J, Chen Z, Li G, Zheng Z, Qiu S, Luo J, Ye C, Zhu S, Zhong N, China Medical Treatment Expert Group for Covid-19. 2020. Clinical Characteristics of Coronavirus Disease 2019 in China. N Engl J Med 382:1708–1720. https://doi.org/10.1056/NEJMoa2002032.
6. Lin L, Jiang X, Zhang Z, Huang S, Zhang Z, Fang Z, Gu Z, Gao L, Shi H, Mai L, Liu Y, Lin X, Lai R, Yan Z, Li X, Shan H. 2020. Gastrointestinal symptoms of 95 cases with SARS-CoV-2 infection. Gut 69:997–1001. https://doi.org/10.1136/gutjnl-2020-321013.
7. Livanos AE, Jha D, Cossarini F, Gonzalez-Reiche AS, Tokuyama M, Aydillo T, Parigi TL, Ladinsky MS, Ramos I, Dunleavy K, Lee B, Dixon RE, Chen ST, Martinez-Delgado G, Nagula S, Bruce EA, Ko HM, Glicksberg BS, Nadkarni G, Pujadas E, Reidy J, Naymagon S, Grinspan A, Ahmad J, Tankelevich M, Bram Y, Gordon R, Sharma K, Houldsworth J, Britton GJ, Chen-Liaw A, Spindler MP, Plitt T, Wang P, Cerutti A, Faith JJ, Colombel JF, Kenigsberg E, Argmann C, Merad M, Gnjatic S, Harpaz N, Danese S, Cordon-Cardo C, Rahman A, Schwartz RE, Kumta NA, Aghemo A, Bjorkman PJ, Petralia F, van Bakel H, Garcia-Sastre A, et al. 2021. Intestinal host response to SARS-CoV-2 infection and COVID-19 outcomes in patients with gastrointestinal symptoms. Gastroenterology 160:2435–2450. https://doi.org/10.1053/j.gastro.2021.02.056.
8. Wölfel R, Corman VM, Guggemos W, Seilmaier M, Zange S, Müller MA, Niemeyer D, Jones TC, Vollmar P, Rothe C, Hoelscher M, Bleicker T, Brünink S, Schneider J, Ehmann R, Zwirglmaier K, Drosten C, Wendtner C. 2020. Virological assessment of hospitalized patients with COVID-2019. Nature. https://doi.org/10.1038/s41586-020-2196-x.
9. Wu Y, Guo C, Tang L, Hong Z, Zhou J, Dong X, Yin H, Xiao Q, Tang Y, Qu X, Kuang L, Fang X, Mishra N, Lu J, Shan H, Jiang G, Huang X. 2020. Prolonged presence of SARS-CoV-2 viral RNA in faecal samples. Lancet Gastroenterol Hepatol 5:434–435. https://doi.org/10.1016/S2468-1253(20)30083-2.
10. Xiao F, Tang M, Zheng X, Liu Y, Li X, Shan H. 2020. Evidence for Gastrointestinal Infection of SARS-CoV-2. Gastroenterology 158:1831–1833.e3. https://doi.org/10.1053/j.gastro.2020.02.055.
11. Xing YH, Ni W, Wu Q, Li WJ, Li GJ, Di Wang W, Tong JN, Song XF, Wing-Kin Wong G, Xing QS. 2020. Prolonged viral shedding in feces of pediatric patients with coronavirus disease 2019. J Microbiol Immunol Infect 53:473–480. https://doi.org/10.1016/j.jmii.2020.03.021.
12. Xu Y, Li X, Zhu B, Liang H, Fang C, Gong Y, Guo Q, Sun X, Zhao D, Shen J, Zhang H, Liu H, Xia H, Tang J, Zhang K, Gong S. 2020. Characteristics of pediatric SARS-CoV-2 infection and potential evidence for persistent fecal viral shedding. Nat Med 26:502–505. https://doi.org/10.1038/s41591-020-0817-4.
13. Guo M, Tao W, Flavell RA, Zhu S. 2021. Reply to: rectally shed SARS-CoV-2 lacks infectivity: time to rethink faecal–oral transmission? Nat Rev Gastroenterol Hepatol 18:669–670. https://doi.org/10.1038/s41575-021-00503-8.
14. Lehmann M, Allers K, Heldt C, Meinhardt J, Schmidt F, Rodriguez-Sillke Y, Kunkel D, Schumann M, Böttcher C, Stahl-Hennig C, Elezkurtaj S, Bojarski C, Radbruch H, Corman VM, Schneider T, Loddenkemper C, Moos V, Weidinger C, Kühl AA, Siegmund B. 2021. Human small intestinal infection by SARS-CoV-2 is characterized by a mucosal infiltration with activated $CD8^+$ T cells. Mucosal Immunol 14:1381–1392. https://doi.org/10.1038/s41385-021-00437-z.
15. Lamers MM, Beumer J, Van Der Vaart J, Knoops K, Puschhof J, Breugem TI, Ravelli RBG, Schayck JP, Van Mykytyn AZ, Duimel HQ, Donselaar E, Van Riesebosch S, Kuijpers HJH, Schipper D, De Wetering WJV, Graaf M, De Koopmans M, Cuppen E, Peters PJ, Haagmans BL, Clevers H. 2020. SARS-CoV-2 productively infects human gut enterocytes. Science. https://doi.org/10.1126/science.abc1669.
16. Stanifer ML, Guo C, Doldan P, Boulant S. 2020. Importance of type I and III interferons at respiratory and intestinal barrier surfaces. Front Immunol.

17. Triana S, Metz-Zumaran C, Ramirez C, Kee C, Doldan P, Shahraz M, Schraivogel D, Gschwind AR, Sharma AK, Steinmetz LM, Herrmann C, Alexandrov T, Boulant S, Stanifer ML. 2021. Single-cell analyses reveal SARS-CoV-2 interference with intrinsic immune response in the human gut. Mol Syst Biol 17. https://doi.org/10.15252/msb.202110232.
18. Zang R, Castro MFG, McCune BT, Zeng Q, Rothlauf PW, Sonnek NM, Liu Z, Brulois KF, Wang X, Greenberg HB, Diamond MS, Ciorba MA, Whelan SPJ, Ding S. 2020. TMPRSS2 and TMPRSS4 promote SARS-CoV-2 infection of human small intestinal enterocytes. Sci Immunol 5:eabc3582. https://doi.org/10.1126/sciimmunol.abc3582.
19. Stanifer ML, Pervolaraki K, Boulant S. 2019. Differential regulation of type I and type III interferon signaling. Int J Mol Sci 20:1445. https://doi.org/10.3390/ijms20061445.
20. Dionne KR, Galvin JM, Schittone SA, Clarke P, Tyler KL. 2011. Type I interferon signaling limits reoviral tropism within the brain and prevents lethal systemic infection. J Neurovirol 17:314–326. https://doi.org/10.1007/s13365-011-0038-1.
21. Pott J, Mahlakõiv T, Mordstein M, Duerr CU, Michiels T, Stockinger S, Staeheli P, Hornef MW. 2011. IFN-λ determines the intestinal epithelial antiviral host defense. Proc Natl Acad Sci U S A 108:7944–7949. https://doi.org/10.1073/pnas.1100552108.
22. Weber E, Finsterbusch K, Lindquist R, Nair S, Lienenklaus S, Gekara NO, Janik D, Weiss S, Kalinke U, Overby AK, Kroger A. 2014. Type I interferon protects mice from fatal neurotropic infection with Langat virus by systemic and local antiviral responses. J Virol 88:12202–12212. https://doi.org/10.1128/JVI.01215-14.
23. Pott J, Stockinger S. 2017. Type I and III interferon in the gut: tight balance between host protection and immunopathology. Front Immunol 8:258. https://doi.org/10.3389/fimmu.2017.00258.
24. Nice TJ, Baldridge MT, McCune BT, Norman JM, Lazear HM, Artyomov M, Diamond MS, Virgin HW. 2015. Interferon-λ cures persistent murine norovirus infection in the absence of adaptive immunity. Science 347:269–273. https://doi.org/10.1126/science.1258100.
25. Baldridge MT, Nice TJ, McCune BT, Yokoyama CC, Kambal A, Wheadon M, Diamond MS, Ivanova Y, Artyomov M, Virgin HW. 2015. Commensal microbes and interferon-λ determine persistence of enteric murine norovirus infection. Science 347:266–269. https://doi.org/10.1126/science.1258025.
26. Mahlakõiv T, Hernandez P, Gronke K, Diefenbach A, Staeheli P. 2015. Leukocyte-derived IFN-α/β and epithelial IFN-λ constitute a compartmentalized mucosal defense system that restricts enteric virus infections. PLoS Pathog 11:e1004782. https://doi.org/10.1371/journal.ppat.1004782.
27. Klinkhammer J, Schnepf D, Ye L, Schwaderlapp M, Gad HH, Hartmann R, Garcin D, Mahlakõiv T, Staeheli P. 2018. IFN-λ prevents influenza virus spread from the upper airways to the lungs and limits virus transmission. Elife 7. https://doi.org/10.7554/eLife.33354.
28. Luker GD, Prior JL, Song J, Pica CM, Leib DA. 2003. Bioluminescence imaging reveals systemic dissemination of herpes simplex virus type 1 in the absence of interferon receptors. J Virol 77:11082–11093. https://doi.org/10.1128/jvi.77.20.11082-11093.2003.
29. Pervolaraki K, Rastgou Talemi S, Albrecht D, Bormann F, Bamford C, Mendoza JL, Garcia KC, McLauchlan J, Höfer T, Stanifer ML, Boulant S. 2018. Differential induction of interferon stimulated genes between type I and type III interferons is independent of interferon receptor abundance. PLoS Pathog 14:e1007420. https://doi.org/10.1371/journal.ppat.1007420.
30. Pervolaraki K, Stanifer ML, Münchau S, Renn LA, Albrecht D, Kurzhals S, Senís E, Grimm D, Schröder-Braunstein J, Rabin RL, Boulant S. 2017. Type I and type III interferons display different dependency on mitogen-activated protein kinases to mount an antiviral state in the human gut. Front Immunol 8:459. https://doi.org/10.3389/fimmu.2017.00459.
31. Stanifer ML, Kee C, Cortese M, Alexandrov T, Bartenschlager R, Boulant S, Zumaran CM, Triana S, Mukenhirn M, Kraeusslich H-G. 2020. Critical role of type III interferon in controlling SARS-CoV-2 infection in human intestinal epithelial cells. Cell Rep 32:107863. https://doi.org/10.1016/j.celrep.2020.107863.
32. Crotta S, Davidson S, Mahlakoiv T, Desmet CJ, Buckwalter MR, Albert ML, Staeheli P, Wack A. 2013. Type I and type III interferons drive redundant amplification loops to induce a transcriptional signature in influenza-infected airway epithelia. PLoS Pathog 9:e1003773. https://doi.org/10.1371/journal.ppat.1003773.
33. Desai N, Neyaz A, Szabolcs A, Shih AR, Chen JH, Thapar V, Nieman LT, Solovyov A, Mehta A, Lieb DJ, Kulkarni AS, Jaicks C, Xu KH, Raabe MJ, Pinto CJ, Juric D, Chebib I, Colvin RB, Kim AY, Monroe R, Warren SE, Danaher P, Reeves JW, Gong J, Rueckert EH, Greenbaum BD, Hacohen N, Lagana SM, Rivera MN, Sholl LM, Stone JR, Ting DT, Deshpande V. 2020. Temporal and spatial heterogeneity of host response to SARS-CoV-2 pulmonary infection. Nat Commun 11. https://doi.org/10.1038/s41467-020-20139-7.
34. Katsura H, Sontake V, Tata A, Kobayashi Y, Edwards CE, Heaton BE, Konkimalla A, Asakura T, Mikami Y, Fritch EJ, Lee PJ, Heaton NS, Boucher RC, Randell SH, Baric RS, Tata PR. 2020. Human lung stem cell-based alveolospheres provide insights into SARS-CoV-2-mediated interferon responses and pneumocyte dysfunction. Cell Stem Cell 27:890–904. https://doi.org/10.1016/j.stem.2020.10.005.
35. Blanco-Melo D, Nilsson-Payant BE, Liu WC, Uhl S, Hoagland D, Møller R, Jordan TX, Oishi K, Panis M, Sachs D, Wang TT, Schwartz RE, Lim JK, Albrecht RA, tenOever BR. 2020. Imbalanced host response to SARS-CoV-2 drives development of COVID-19. Cell 181:1036–1045.e9. https://doi.org/10.1016/j.cell.2020.04.026.
36. Chu H, Chan JFW, Wang Y, Yuen TTT, Chai Y, Shuai H, Yang D, Hu B, Huang X, Zhang X, Hou Y, Cai JP, Zhang AJ, Zhou J, Yuan S, To KKW, Hung IFN, Cheung TT, Ng ATL, Hau-Yee Chan I, Wong IYH, Law SYK, Foo DCC, Leung WK, Yuen KY. 2021. SARS-CoV-2 induces a more robust innate immune response and replicates less efficiently than SARS-CoV in the human intestines: an *ex vivo* study with implications on pathogenesis of COVID-19. Cell Mol Gastroenterol Hepatol 11:771–781. https://doi.org/10.1016/j.jcmgh.2020.09.017.
37. Shuai H, Chu H, Hou Y, Yang D, Wang Y, Hu B, Huang X, Zhang X, Chai Y, Cai JP, Chan JFW, Yuen KY. 2020. Differential immune activation profile of SARS-CoV-2 and SARS-CoV infection in human lung and intestinal cells: implications for treatment with IFN-β and IFN inducer. J Infect 81:e1–e10. https://doi.org/10.1016/j.jinf.2020.07.016.
38. Vanderheiden A, Ralfs P, Chirkova T, Upadhyay AA, Zimmerman MG, Bedoya S, Aoued H, Tharp GM, Pellegrini KL, Manfredi C, Sorscher E, Mainou B, Lobby JL, Kohlmeier JE, Lowen AC, Shi P-Y, Menachery VD, Anderson LJ, Grakoui A, Bosinger SE, Suthar MS. 2020. Type I and type III interferons restrict SARS-CoV-2 infection of human airway epithelial cultures. J Virol 94:e00985-20. https://doi.org/10.1128/JVI.00985-20.
39. Meffre E, Iwasaki A. 2020. Interferon deficiency can lead to severe COVID. Nature 587:374–376. https://doi.org/10.1038/d41586-020-03070-1.
40. Felgenhauer U, Schoen A, Gad HH, Hartmann R, Schaubmar AR, Failing K, Drosten C, Weber F. 2020. Inhibition of SARS–CoV-2 by type I and type III interferons. J Biol Chem 295:13958–13964. https://doi.org/10.1074/jbc.AC120.013788.
41. Park A, Iwasaki A. 2020. Type I and type III interferons: induction, signaling, evasion, and application to combat COVID-19. Cell Host Microbe 27:870–878. https://doi.org/10.1016/j.chom.2020.05.008.
42. Rebendenne A, Chaves Valadão AL, Tauziet M, Maarifi G, Bonaventure B, McKellar J, Planès R, Nisole S, Arnaud-Arnould M, Moncorgé O, Goujon C. 2021. SARS-CoV-2 triggers an MDA-5-dependent interferon response which is unable to control replication in lung epithelial cells. J Virol 95:e02415-20. https://doi.org/10.1128/JVI.02415-20.
43. Busnadiego I, Fernbach S, Pohl MO, Karakus U, Huber M, Trkola A, Stertz S, Hale BG. 2020. Antiviral activity of type I, II, and III interferons counterbalances *ace2* inducibility and restricts sars-cov-2. mBio 11:e01928-20. https://doi.org/10.1128/mBio.01928-20.
44. Chu H, Chan JFW, Wang Y, Yuen TTT, Chai Y, Hou Y, Shuai H, Yang D, Hu B, Huang X, Zhang X, Cai JP, Zhou J, Yuan S, Kok KH, To KKW, Chan IHY, Zhang AJ, Sit KY, Au WK, Yuen KY. 2020. Comparative replication and immune activation profiles of SARS-CoV-2 and SARS-CoV in human lungs: an *ex vivo* study with implications for the pathogenesis of COVID-19. Clin Infect Dis 71:1400–1409. https://doi.org/10.1093/cid/ciaa410.
45. Munis AM, Bentley EM, Takeuchi Y. 2020. A tool with many applications: vesicular stomatitis virus in research and medicine. Expert Opin Biol Ther 20:1187–1201. https://doi.org/10.1080/14712598.2020.1787981.
46. Bhushal S, Wolfsmüller M, Selvakumar TA, Kemper L, Wirth D, Hornef MW, Hauser H, Köster M. 2017. Cell polarization and epigenetic status shape the heterogeneous response to type III interferons in intestinal epithelial cells. Front Immunol 8:761.
47. Marcello T, Grakoui A, Barba-Spaeth G, Machlin ES, Kotenko SV, Macdonald MR, Rice CM. 2006. Interferons α and λ Inhibit Hepatitis C Virus Replication With Distinct Signal Transduction and Gene Regulation Kinetics. Gastroenterology 131:1887–1898. https://doi.org/10.1053/j.gastro.2006.09.052.
48. Meager A, Visvalingam K, Dilger P, Bryan D, Wadhwa M. 2005. Biological activity of interleukins-28 and -29: comparison with type I interferons. Cytokine 31:109–118. https://doi.org/10.1016/j.cyto.2005.04.003.
49. Kohli A, Zhang X, Yang J, Russell RS, Donnelly RP, Sheikh F, Sherman A, Young H, Imamichi T, Lempicki RA, Masur H, Kottilil S. 2012. Distinct and overlapping genomic profiles and antiviral effects of interferon-λ and -α

On HCV-infected and noninfected hepatoma cells. J Viral Hepat 19:843–853. https://doi.org/10.1111/j.1365-2893.2012.01610.x.
50. Sheppard P, Kindsvogel W, Xu W, Henderson K, Schlutsmeyer S, Whitmore TE, Kuestner R, Garrigues U, Birks C, Roraback J, Ostrander C, Dong D, Shin J, Presnell S, Fox B, Haldeman B, Cooper E, Taft D, Gilbert T, Grant FJ, Tackett M, Krivan W, McKnight G, Clegg C, Foster D, Klucher KM. 2003. IL-28, IL-29, and their class II cytokine receptor IL-28R. Nat Immunol 4:63–68. https://doi.org/10.1038/ni873.
51. Trypsteen W, Van Cleemput J, van Snippenberg W, Gerlo S, Vandekerckhove L. 2020. On the whereabouts of SARS-CoV-2 in the human body: a systematic review. PLoS Pathog 16:e1009037. https://doi.org/10.1371/journal.ppat.1009037.
52. Remmelink M, De Mendonça R, D'Haene N, De Clercq S, Verocq C, Lebrun L, Lavis P, Racu ML, Trépant AL, Maris C, Rorive S, Goffard JC, De Witte O, Peluso L, Vincent JL, Decaestecker C, Taccone FS, Salmon I. 2020. Unspecific post-mortem findings despite multiorgan viral spread in COVID-19 patients. Crit Care 24. https://doi.org/10.1186/s13054-020-03218-5.
53. Tavazzi G, Pellegrini C, Maurelli M, Belliato M, Sciutti F, Bottazzi A, Sepe PA, Resasco T, Camporotondo R, Bruno R, Baldanti F, Paolucci S, Pelenghi S, Iotti GA, Mojoli F, Arbustini E. 2020. Myocardial localization of coronavirus in COVID-19 cardiogenic shock. Eur J Heart Fail 22:911–915. https://doi.org/10.1002/ejhf.1828.
54. Bradley BT, Maioli H, Johnston R, Chaudhry I, Fink SL, Xu H, Najafian B, Deutsch G, Lacy JM, Williams T, Yarid N, Marshall DA. 2020. Histopathology and ultrastructural findings of fatal COVID-19 infections in Washington State: a case series. Lancet 396:320–332. https://doi.org/10.1016/S0140-6736(20)31305-2.
55. Puelles VG, Lütgehetmann M, Lindenmeyer MT, Sperhake JP, Wong MN, Allweiss L, Chilla S, Heinemann A, Wanner N, Liu S, Braun F, Lu S, Pfefferle S, Schröder AS, Edler C, Gross O, Glatzel M, Wichmann D, Wiech T, Kluge S, Pueschel K, Aepfelbacher M, Huber TB. 2020. Multiorgan and renal tropism of SARS-CoV-2. N Engl J Med 383. https://doi.org/10.1056/NEJMc2011400.
56. Schaller T, Hirschbühl K, Burkhardt K, Braun G, Trepel M, Märkl B, Claus R. 2020. Postmortem examination of patients with COVID-19. JAMA 323:2518. https://doi.org/10.1001/jama.2020.8907.
57. Israelow B, Song E, Mao T, Lu P, Meir A, Liu F, Alfajaro MM, Wei J, Dong H, Homer RJ, Ring A, Wilen CB, Iwasaki A. 2020. Mouse model of SARS-CoV-2 reveals inflammatory role of type i interferon signaling. J Exp Med 217:e20201241. https://doi.org/10.1084/jem.20201241.
58. V'kovski P, Kratzel A, Steiner S, Stalder H, Thiel V. 2021. Coronavirus biology and replication: implications for SARS-CoV-2. Nat Rev Microbiol 19:155–170. https://doi.org/10.1038/s41579-020-00468-6.
59. Coccia EM, Krust B, Hovanessian AG. 1994. Specific inhibition of viral protein synthesis in HIV-infected cells in response to interferon treatment. J Biol Chem 269:23087–23094. https://doi.org/10.1016/S0021-9258(17)31623-X.
60. Diamond MS, Harris E. 2001. Interferon inhibits dengue virus infection by preventing translation of viral RNA through a PKR-independent mechanism. Virology 289:297–311. https://doi.org/10.1006/viro.2001.1114.
61. Sadler AJ, Williams BRG. 2008. Interferon-inducible antiviral effectors. Nat Rev Immunol. https://doi.org/10.1038/nri2314.
62. Diamond MS, Farzan M. 2013. The broad-spectrum antiviral functions of IFIT and IFITM proteins. Nat Rev Immunol. Nat. Nat Rev Immunol 13:46–57. https://doi.org/10.1038/nri3344.
63. Vladimer GI, Górna MW, Superti-Furga G. 2014. IFITs: emerging roles as key anti-viral proteins. Front Immunol 5:94. https://doi.org/10.3389/fimmu.2014.00094.
64. Wu N, Nguyen XN, Wang L, Appourchaux R, Zhang C, Panthu B, Gruffat H, Journo C, Alais S, Qin J, Zhang N, Tartour K, Catez F, Mahieux R, Ohlmann T, Liu M, Du B, Cimarelli A. 2019. The interferon stimulated gene 20 protein (ISG20) is an innate defense antiviral factor that discriminates self versus non-self translation. PLoS Pathog 15:e1008093. https://doi.org/10.1371/journal.ppat.1008093.
65. Selvakumar TA, Bhushal S, Kalinke U, Wirth D, Hauser H, Köster M, Hornef MW. 2017. Identification of a predominantly interferon-λ-induced transcriptional profile in murine intestinal epithelial cells. Front Immunol 8:1302. https://doi.org/10.3389/fimmu.2017.01302.
66. Jilg N, Lin W, Hong J, Schaefer EA, Wolski D, Meixong J, Goto K, Brisac C, Chusri P, Fusco DN, Chevaliez S, Luther J, Kumthip K, Urban TJ, Peng LF, Lauer GM, Chung RT. 2014. Kinetic differences in the induction of interferon stimulated genes by interferon-α and interleukin 28B are altered by infection with hepatitis C virus. Hepatology 59:1250–1261. https://doi.org/10.1002/hep.26653.
67. Voigt EA, Yin J. 2015. Kinetic differences and synergistic antiviral effects between type I and type III interferon signaling indicate pathway independence. J Interferon Cytokine Res 35:734–747. https://doi.org/10.1089/jir.2015.0008.
68. Zhou Z, Hamming OJ, Ank N, Paludan SR, Nielsen AL, Hartmann R. 2007. Type III interferon (IFN) induces a type I IFN-like response in a restricted subset of cells through signaling pathways involving both the Jak-STAT pathway and the mitogen-activated protein kinases. J Virol 81:7749–7758. https://doi.org/10.1128/JVI.02438-06.
69. Da Lin J, Feng N, Sen A, Balan M, Tseng HC, McElrath C, Smirnov SV, Peng J, Yasukawa LL, Durbin RK, Durbin JE, Greenberg HB, Kotenko SV. 2016. Distinct roles of type I and type III interferons in intestinal immunity to homologous and heterologous rotavirus infections. PLoS Pathog 12:e1005726. https://doi.org/10.1371/journal.ppat.1005726.
70. Cinatl J, Morgenstern B, Bauer G, Chandra P, Rabenau H, Doerr HW. 2003. Treatment of SARS with human interferons. Lancet 362:293–294. https://doi.org/10.1016/S0140-6736(03)13973-6.
71. Arabi YM, Mandourah Y, Al-Hameed F, Sindi AA, Almekhlafi GA, Hussein MA, Jose J, Pinto R, Al-Omari A, Kharaba A, Almotairi A, Al Khatib K, Alraddadi B, Shalhoub S, Abdulmomen A, Qushmaq I, Mady A, Mady O, Al-Aithan AM, Al-Raddadi R, Ragab A, Balkhy HH, Balkhy A, Deeb AM, Al Mutairi H, Al-Dawood A, Merson L, Hayden FG, Fowler RA, Saudi Critical Care Trial Group. 2018. Corticosteroid therapy for critically ill patients with middle east respiratory syndrome. Am J Respir Crit Care Med 197:757–767. https://doi.org/10.1164/rccm.201706-1172OC.
72. Arabi YM, Asiri AY, Assiri AM, Balkhy HH, Al Bshabshe A, Al Jeraisy M, Mandourah Y, Azzam MHA, Bin Eshaq AM, Al Johani S, Al Harbi S, Jokhdar HAA, Deeb AM, Memish ZA, Jose J, Ghazal S, Al Faraj S, Al Mekhlafi GA, Sherbeeni NM, Elzein FE, Al-Hameed F, Al Saedi A, Alharbi NK, Fowler RA, Hayden FG, Al-Dawood A, Abdelzaher M, Bajhmom W, AlMutairi BM, Hussein MA, Alothman A, Saudi Critical Care Trials Group. 2020. Interferon β-1b and lopinavir–ritonavir for Middle East respiratory syndrome. N Engl J Med 383:1645–1656. https://doi.org/10.1056/NEJMoa2015294.
73. Sallard E, Lescure FX, Yazdanpanah Y, Mentre F, Peiffer-Smadja N. 2020. Type 1 interferons as a potential treatment against COVID-19. Antiviral Res 178:104791. https://doi.org/10.1016/j.antiviral.2020.104791.
74. Lokugamage KG, Hage A, de Vries M, Valero-Jimenez AM, Schindewolf C, Dittmann M, Rajsbaum R, Menachery VD. 2020. Type I interferon susceptibility distinguishes SARS-CoV-2 from SARS-CoV. bioRxiv. https://www.biorxiv.org/content/10.1101/2020.03.07.982264v4.
75. Hung IFN, Lung KC, Tso EYK, Liu R, Chung TWH, Chu MY, Ng YY, Lo J, Chan J, Tam AR, Shum HP, Chan V, Wu AKL, Sin KM, Leung WS, Law WL, Lung DC, Sin S, Yeung P, Yip CCY, Zhang RR, Fung AYF, Yan EYW, Leung KH, Ip JD, Chu AWH, Chan WM, Ng ACK, Lee R, Fung K, Yeung A, Wu TC, Chan JWM, Yan WW, Chan WM, Chan JFW, Lie AKW, Tsang OTY, Cheng VCC, Que TL, Lau CS, Chan KH, To KKW, Yuen KY. 2020. Triple combination of interferon beta-1b, lopinavir–ritonavir, and ribavirin in the treatment of patients admitted to hospital with COVID-19: an open-label, randomised, phase 2 trial. Lancet 395:1695–1704. https://doi.org/10.1016/S0140-6736(20)31042-4.
76. Clementi N, Ferrarese R, Criscuolo E, Diotti RA, Castelli M, Scagnolari C, Burioni R, Antonelli G, Clementi M, Mancini N. 2020. Interferon-β-1a inhibition of severe acute respiratory syndrome-coronavirus 2 *in vitro* when administered after virus infection. J Infect Dis 222:722–725. https://doi.org/10.1093/infdis/jiaa350.
77. Biggioggero M, Gabbriellini L, Meroni PL. 2010. Type I interferon therapy and its role in autoimmunity, p 248–254. *In* Autoimmunity. Taylor & Francis, New York, NY. https://doi.org/10.3109/08916930903510971.